



Highly advanced Probabilistic design and Enhanced Reliability methods for high-value, cost-efficient offshore WIND

Title: Electrical grid model
Deliverable no: D5.2

Delivery date: 14.03.2023
Lead beneficiary: EPRI
Dissemination level: Public



This project has received funding from the European Union's Horizon 2020 Research and Innovation Programme under Grant Agreement No. 101006689



Contents

1. Executive Summary	2
2. Introduction and Overview	3
3. Type 3-4 General description.....	3
3.1. Type 3 Description.....	4
3.2. Type 4 Description.....	5
4. Grid disturbances	6
4.1. Low Voltage Ride Through (LVRT)	7
5. Teesside Turbine description	9
5.1. ABB Generator description.....	10
5.2. Teesside Observed events	11
6. Teesside Integrated Mechanical/Electrical framework	12
6.1. Electrical model components	13
6.2. Generator.....	14
6.3. Back-to-Back converter	16
6.4. Electric Grid.....	20
6.5. Mechanical model components.....	22
7. LVRT Time domain Simulations.....	23
8. Results.....	28
8.1. DLC 2.4 Power production with loss of electrical network.....	28
8.2. DLC 2.5 Power production with Low Voltage Ride Through.....	34
8.2.1. Allowable bearing static equivalent load during LVRT	35
8.3. Combining Low Voltage Ride Through events with normal production load cases	37
9. Discussion	39
10. Conclusion	40
11. Outlook	41
Bibliography	42
Appendix A.....	44
Appendix B.....	46



List of Abbreviations

PCC	Point of common coupling
DC	Direct Current
DFIG	Doubly-Fed Induction Generator
GC	Grid Code
IGBT	Insulated Gate Bipolar Thyristor
LVRT	Low Voltage ride through
TSO	Transmission system Operator
WF	Wind Farm
WTG	Wind Turbine Generator



1. Executive Summary

This work package aims to evaluate the fatigue of mechanical components in the wind turbine resulting from exposure to a series of grid disturbances throughout its operational life. Based on historical data from a specific site, statistical analysis, and numerical models of the mechanical and electrical components, an estimate of the remaining lifetime is calculated.

To create the numerical model for the turbines, an extensive literature review has been conducted, taking into consideration several grid connection requirements from different countries, resulting in a detailed electro-mechanical model that includes all relevant control systems necessary to comply with these requirements.

2. Introduction and Overview

Throughout the operational lifetime of a wind turbine generator (WTG), the mechanical structure and electrical system must endure various types of disturbances. Perturbations in the grid are caused by different phenomena and can disrupt power transmission to the grid.

These disturbances can cause significant changes in voltage, frequency, and current values, resulting in electromagnetic transients in the connected WTG. The changes can also affect the torque and speed of the WTG, which can lead to modified loads and cycling loads in the structure. The degree to which grid perturbations impact the loads depends on the type of WTG, which primarily refers to the technology used to transfer energy to the grid.

Modern power electronic devices such as back-to-back converters play a crucial role in mitigating the impact of disturbances on the mechanical structure. Chapter 3 provides a detailed description of WTG types and their influence on the analysis.

Grid disturbances can stem from various sources, ranging from natural disasters to electrical malfunctions, and can cause different types of perturbations in the grid. Chapter 4 includes a brief discussion on grid phenomena and their implications on electric transients.

Each country's grid codes regulate how a wind turbine generator (WTG) responds to disturbances in the grid. These codes establish minimum performance requirements in terms of power injection, as well as frequency or voltage support. The WTG's response to grid transients can result in additional demands on the electrical system and structure. Chapter 4.1 provides an overview of some of these requirements.

In Chapters 6 and 7, the integrated framework used in this work package is discussed in detail. The model was created to serve as a tool for calculating the loads resulting from grid disturbances, taking into account all previous analyses and integrating them.

The final chapters of this report present the results of simulations and subsequent analysis. A dedicated chapter provides a final discussion on the accuracy of these results compared to previous studies found in the literature.

3. Type 3-4 General description

Modern wind turbines for utility scale applications use the horizontal axis technology with typical ratings in the range of 500 kW to 6MW. The technology employed by these turbines can vary according to each manufacturer. However, a common classification of this is often described as follows [1].

- Type 1: Fixed-speed wind turbines
- Type 2: Variable-slip wind turbines
- Type 3: Doubly fed induction generator (DFIG) wind turbine
- Type 4: Full-converter wind turbines

Although types 1 and 2 have proven to be robust and reliable design, type 3 and 4 have coped market shares in the recent years due to its capacity of operating at variable speed and the capacity of providing reactive power compensation. This allows them to operate at a maximum power extraction point while providing grid support. Therefore, this section will mainly concentrate on this last two technologies.

3.1. Type 3 Description

The type 3 WTG also commonly referred as the Double Fed Induction Generator (DFIG), is technological evolution of types 1 and 2. The DFIG is based on an induction generator where the stator windings are directly connected to the grid through a transformer, while the rotor is connected to a back-to-back converter via slip rings, this way, the rotor frequency can differ from the grid frequency. The converter's other side is also connected to the grid through a transformer.

By using the converter, P (active power) and Q (reactive power) can be controlled independently from the generator's rotor speed (see Figure 1). However, due to maximal rotor slip limitations, rotor speed will have a minimum and maximum operation point.

To protect the rotor converter from high currents, a crowbar is also commonly used. In case any excessive voltage is sense by the rotor, the crowbar will short circuit rotor windings to prevent excessive currents in the converter's IGBTs (insulated-gate bipolar transistor).

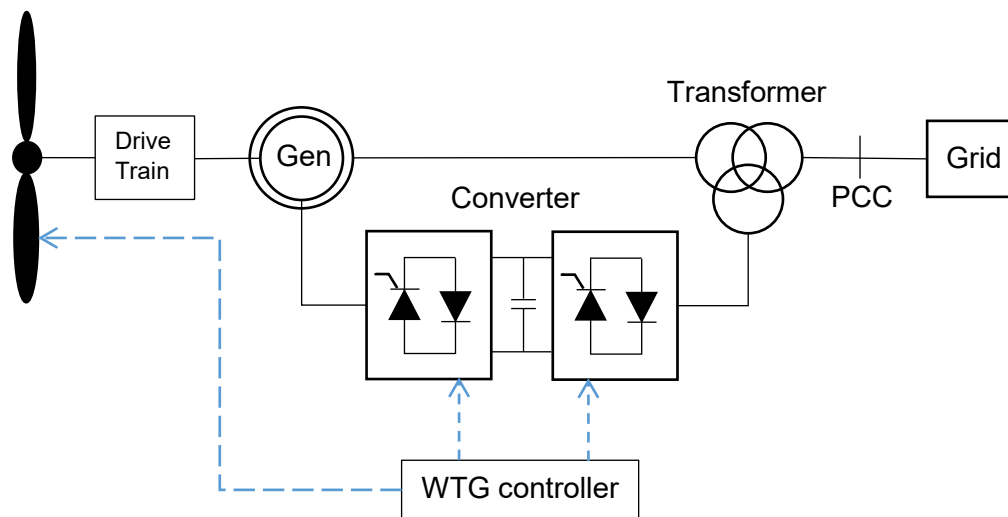


Figure 1 Type 3 WTG simplified diagram

For many years, type 3 WTG have been the technology standard for many manufactures and technology providers around the globe. However, with the upcoming of offshore wind turbines and improved efficiency in power electronics technology, type 4 WTG have started to take bigger shares in the market.

3.2. Type 4 Description

Type 4 WTG is typically named as the Full converter WTG. This technology represents a step change in industry as it out passes all capabilities for all previously mention types.

The full converter technology is based on either synchronous or induction generators. The stator windings and the grid are interconnected through a full rated inverter that decouples the grid dynamics from the generator completely. This allows the generator to operate in asynchrony of the grid frequency and thus, by using variable speed, it can maximize the power output in a larger range of speed.

The current trend for the rotor is to use a permanent magnet alternator which eliminates the necessity of winding in the rotor and. This allows the rotor to operate at lower speeds and eliminates the necessity of a gearbox, thus, increasing the overall efficiency of the design. However, some type 4 WTG design use wound rotor with gearboxes in the drivetrain. This last solution has been extensively used by many vendors in past years (see Figure 2).

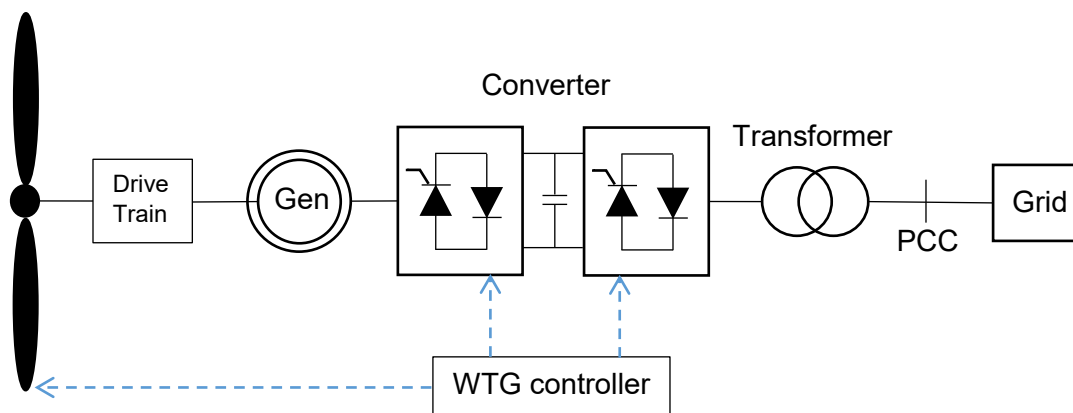


Figure 2 Type IV WTG simplified diagram

Several power electronic architectures can be used in the full converter configuration. The generator side converter can be composed by a rectifier followed by a buck/boost converter to control and limit the DC link voltage and it also can be composed of a full gate bridge with IGBTs. In the last case, the generator side converter is set to control either the generator speed or torque depending on the wind conditions. The grid side converter is set to control the power flow into the grid, and it is normally composed of a full gate bridge with IGBTs. As this side is exposed to grid dynamics, voltage dips can produce large disturbances during normal operation of the converter limiting the power generation [2].

In back-to-back converter operation, a DC chopper is connected in the DC link to limit high excursions in the DC voltage that could potentially damage the capacitors bank [3]. A subproduct of this behavior is that dynamics between grid and generator sides are decoupled as the chopper acts as power sink for the generator side.

The control architecture for the back-to-back converter can have different configurations depending upon main control objectives. One of these configurations is described in [4] where the DC link voltage can be controlled by the generator side instead of the classic view where it is controlled by the grid side. The advantage of this is that the faulted voltage ride through (FVRT) capability is directly integrated as the DC voltage is reduced during the fault. Eventually, this action will decrease power production on the generator side. The control system is explained in-detail in the following chapters of the report.

4. Grid disturbances

Normal grid operation can be interrupted by a series of events of different nature. These events range from natural phenomena to failure of electric devices or equipment on the system. Whenever any of these failures arise, a grid disturbance is generated (see Figure 3).

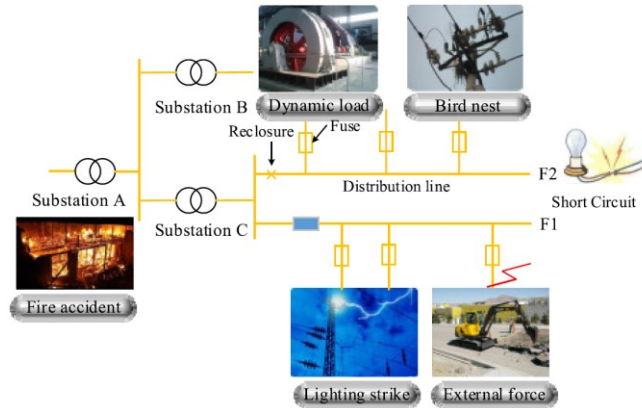


Figure 3 Natural disasters or load transient conditions result in grid voltage sags [5]

When a grid disturbance takes place, the frequency and voltage are disturbed. However, it is important to understand that, depending on the physical nature of the disturbance, frequency or voltage will be affected in different magnitudes.

In normal operation, power generation and load need to be always balanced, if a generation unit trips or load is shed, this balance is lost given as a result a frequency oscillation with less impact over the voltage profile.

In case a short circuit takes place in some part of the grid, the grid impedance is changed as a result. Depending on the impedance to the fault (commonly named as electrical distance) the voltage sag caused by it can be considerable for the units connected in the proximity. In these conditions, the voltage is primarily impacted, but the frequency may also be affected if the voltage sag results in unit outages.

In general, Transmission System Operators (TSO) from different countries addresses these issues by defining the expected behavior that each unit needs to provide whenever these disturbances occur. The set of all requirements are collected in the grid codes (GC). In the following section, some of these requirements are reviewed in more detail.

4.1. Low Voltage Ride Through (LVRT)

The LVRT requirement refers to the capacity of a generation unit to withstand voltage sags in the grid. To describe it, a disconnection zone is delimited by each TSO, which is defined as the area below a voltage profile against time. In Figure 4, LVRT requirements for power plants in different GC specifications [6] is shown.

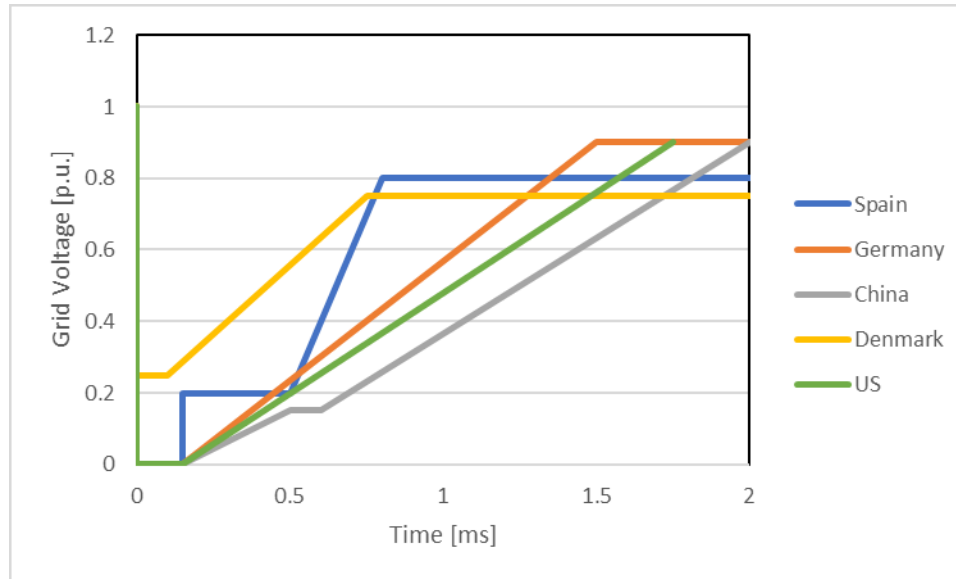


Figure 4 Different Low Voltage Ride Through (LVRT) envelopes according to several Grid Codes (GCs). Reproduced from Ref [6]

When external factors interfere with the electrical isolation, causing current arcs and disrupting the operation of the power grid, a short circuit (SC) is created. There are numerous potential causes of SCs in a grid. Environmental factors, equipment malfunctions, bird nesting along power lines, etc. Any of these situations' effects could result in a grid SC. All of the aforementioned scenarios have the potential to result in a voltage collapse.

The main forms of short circuit are: single-phase to ground short-circuit, two-phase interphase short-circuit, the two-phase to ground short-circuit, and the three-phase grounding short-circuit [7], with a relative probability of about 70%, 15%, 10%, 5% respectively. Understanding the effects that any of these faults will have on the structure is crucial before determining the severity that these represent to the WTG.

If three phase short-circuit rises, the voltage sag is produced in the vicinity of the fault and current is drawn from the sources, but no power can be produced by the absence of potential at fault location. If the fault is located close to the wind farm, it will prevent the turbines from transmitting any power to the grid. This means that produced power will be absorbed by the structure and electric components of the WTG [8].

For single and double-phase SCs the effect will be similar to three phase SC. However, for these faults, the remaining "healthy phases" will be still capable of transmitting power to the grid meaning that only part of the produced power will need to be absorbed by the WTG components while the rest is still evacuated correctly.

Sequence components theory is a useful tool to understand the behavior of the different types of SCs. Under this theory, any 3-phase unbalanced signal can be decomposed into 3 independent and balanced signals: positive, negative and zero sequences. Under normal operation, the grid voltage is balanced and therefore,

it can be described only by a positive sequence. If a fault takes place in 1 or 2 phases, the system becomes unbalanced and therefore, negative and zero sequences are necessary to describe it. A particular situation arrives in the case of 3-phase short-circuits where all 3-phases are equally perturbed. Since the fault is symmetrical across all phases, the system can be still considered as balanced and therefore, it can be modelled as a positive sequence. This means that negative and zero sequence can be neglected.

In Figure 5 shows an example of a 3-phase SC where the voltages at the fault locations are being measured. It can be observed that during the fault, the voltages are still symmetrical although the magnitude has decreased substantially. This shows that even during the fault the voltages remained balanced.

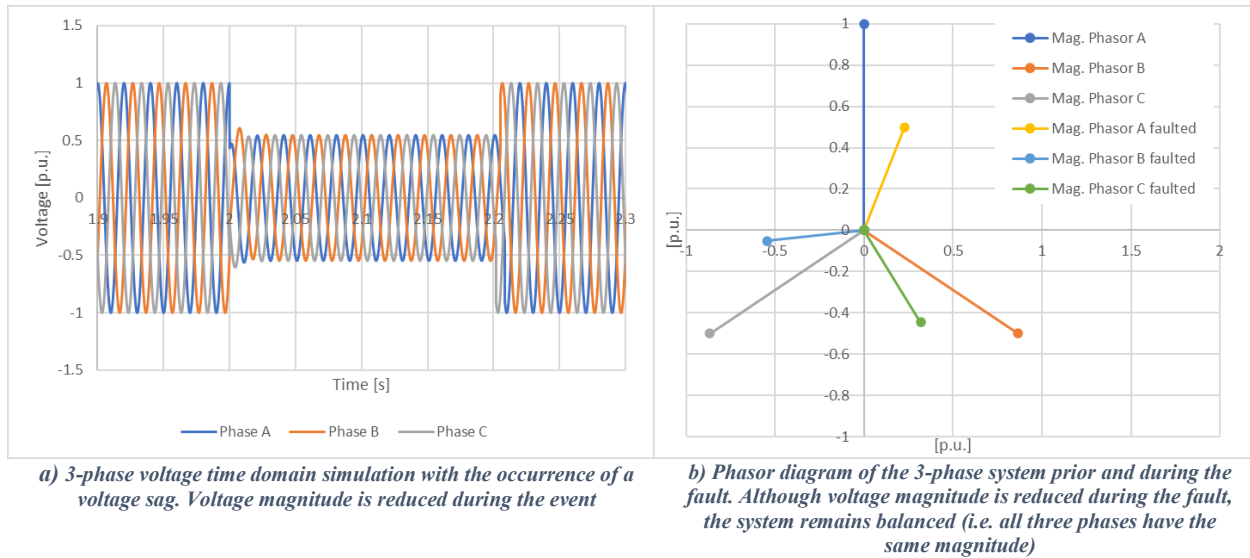


Figure 5 Balance voltage behavior prior the fault and during the fault.

The wind turbine controllers will detect the SC as a sudden reduction in power delivered to the grid, regardless of whether it occurs in one or more phases. Moreover, distinguishing between balanced and unbalanced faults would require dedicated controllers, which may not always be necessary and are beyond the scope of this work. As a result, to estimate the remaining power being supplied to the grid, the voltage sag can be simulated using a three-phase balanced fault with various levels of short-circuit impedance. This approach will be employed in this report and elaborated upon in subsequent sections.

5. Teesside Turbine description

The electro-mechanical modeling and analysis conducted in this report has been based on the available data collected from EDF's Teesside Wind Farm.

Teesside is an offshore wind farm located in the United Kingdom. It is composed by 27 Siemens SWT-2.3-93 turbines with 2.3 MW rated power and 93 m of rotor diameter [9]. The Siemens SWT-2.3-93 generation is based on an asynchronous squirrel cage generator [10]. The grid connection is managed by a full back-to-back NetConverter®.

According to all previously given type descriptions, the current WTG under study falls in the type IV descriptions and therefore, it will be explained in detail in the following sections. This configuration is depicted in the figure below (see Figure 6).

The vendor's description of the model ensures that NetConverter® technology is capable of withstanding different grid disturbances as LVRT events according to different GCs. This means that the WTG has been provided with the necessary hardware and software to withstand this operation. In the following sections, these assumptions will be used to derive the necessary power electronics and control system to cope with this task.

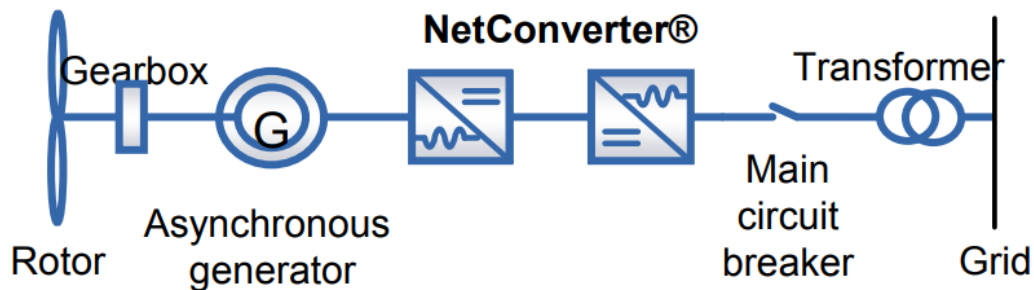


Figure 6 NetConverter diagram reproduced from [11] [12]

5.1. ABB Generator description

As mentioned earlier, Siemens SWT-2.3-93 uses a squirrel cage generator. Our literature research has found that this generator design is provided by ABB [10]. The following table depicts its main features

Table 1 Squirrel cage induction generator parameters. Reproduced from [10]

Parameter	Value
Machine type code	AMA 500L4/6A BAXYH
Machine type	Two speed, squirrel cage generator
Mounting designation	IM 1001
Protected by enclosure	IP 54
Method of cooling	IC 611
Insulation / Temperature rise	Class F / Class B
Standards	IEC
Ambient temperature, max.	50 °C
Cooling air temperature, max.	40 °C
Altitude, max.	1000 m.a.s.l.
Duty type	S1
Rated output	2300kW/2632kVA
Connection of stator winding	Delta
Voltage	690 V
Frequency	50 Hz
Speed	1512 rpm
Current	2174 A
Relat. Starting current	5,2
Relat. Maximum torque	2,4
No load current	584 A
Rated torque	15080 Nm

This data provides enough information to calculate the steady state operation of the turbine given by the speed and wind conditions. However, there is not enough details to derive a practical electrical model to be used in a transient simulation, which is necessary to study grid disturbance response. To achieve this, the equivalent transient and sub-transient impedances would be required.

The general product description also provides information to derive an equivalent synchronous machine model. Although the internal structure and electrical behavior of the synchronous machine differs substantially of the induction generator, this equivalent is an electrical model whose input/output response will match that of the squirrel cage during transient periods.

Given that grid disturbances are essentially a dynamic event, this equivalent synchronous machine is a more suitable model, minded for transient simulations specifically. However, it is important to bear in mind that the result given by this model are not guaranteed as described by manufacture's disclaimer. These parameters are shown in the following Table 2.

Table 2 Equivalent Synchronous machine parameters. Reproduced from [10]

Parameter Name	Symbol	Value
Synchronous reactance (saturated, unsat)	X_d	0.670 0.97
Negative phase sequence synchronous reactance	X_{-}	0.041
Negative phase sequence synchronous resistance	R_{-}	0.003
Positive phase sequence synchronous reactance	X_{+}	0.084
Positive phase sequence synchronous resistance	R_{+}	0.161
Zero phase sequence reactance 2)	X_0	N.A. -
Zero phase sequence resistance 2)	R_0	N.A. -
Direct axis transient open circuit time constant	T'_{d0}	1.519 s
Subtransient open circuit time constant	T''_{d0}	0.013 s
Direct axis transient short circuit time constant	T'_d	0.081 s
Subtransient short circuit time constant	T''_d	0.012 s
Armature time constant	T_a	0.042 s
Locked rotor power factor	-	0.12
Open circuit saturation curve points 3)	$S(1.0)$	1.42
Open circuit saturation curve points 3)	$S(1.2)$	2.24
Inertia constant of generator	H	0.294 kW/s/kVA

5.2. Teesside Observed events

Teesside SCADA data from Jan-2015 to Jan-2019 has been studied in order to find possible grid disturbances occurred during that period. It has been found that the extreme low voltage conditions are being stored per each of the WTGs in the wind farm. To use this information, data has been processed and filter to eliminate values that are far outside of the normal range [13] (this can be caused by sensor failures or SCADA communication errors). The filtered SCADA data with LV events has been summarized in the following Figure 7

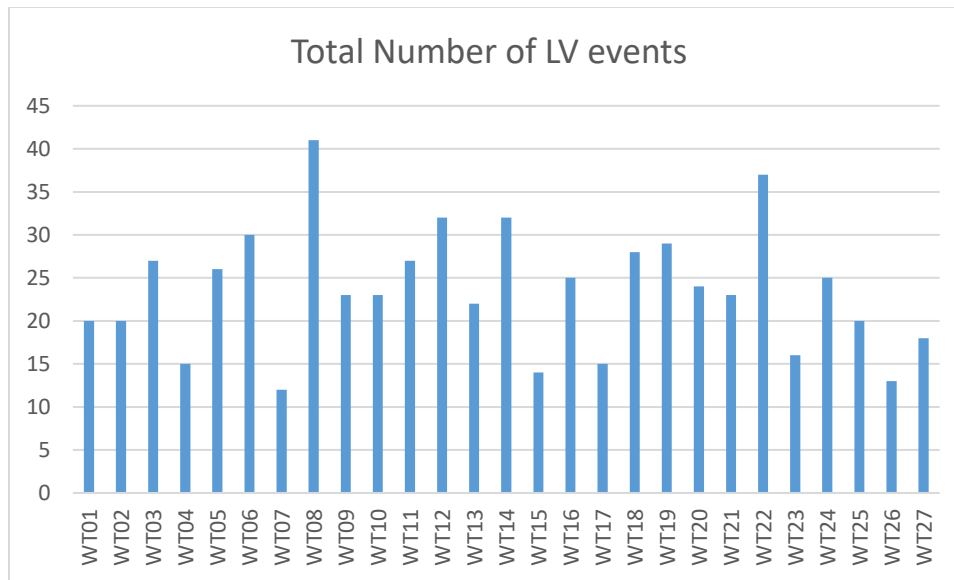


Figure 7 Low Voltage number of events in Teesside WF from Jan-2015 to Jan-2019

From SCADA and events data, there is no possibility of inferring which kind of fault triggered the alarms. As the focus of this report is to assess the impact of grid disturbances on the turbine components, three phase short-circuit faults will be assumed for the rest of the study. As it will be demonstrated later, by assuming this, a worst-case scenario can be constructed and therefore, any other collection of faults will have lesser impact on the structure.

6. Teesside Integrated Mechanical/Electrical framework

As was already mentioned in this document, the GC establishes a LVRT requirement for a grid connected WTG. This requirement demands the capability of remaining grid connected for support both during and after the fault. If the GC is to be followed, this could ultimately be transmitted as additional stress to the structure and blades.

To assess the impact of such a requirement, a joint framework for the mechanical and the electrical systems needs to be created. With this, it should be possible to measure all energy transfers between the electrical and the mechanical systems, and further, the stress over the structure caused by the grid disturbances.

EPRI has developed a model to address this issue by combining mechanical and electrical dynamics into a single framework. This model is shown in detail in Figure 8.

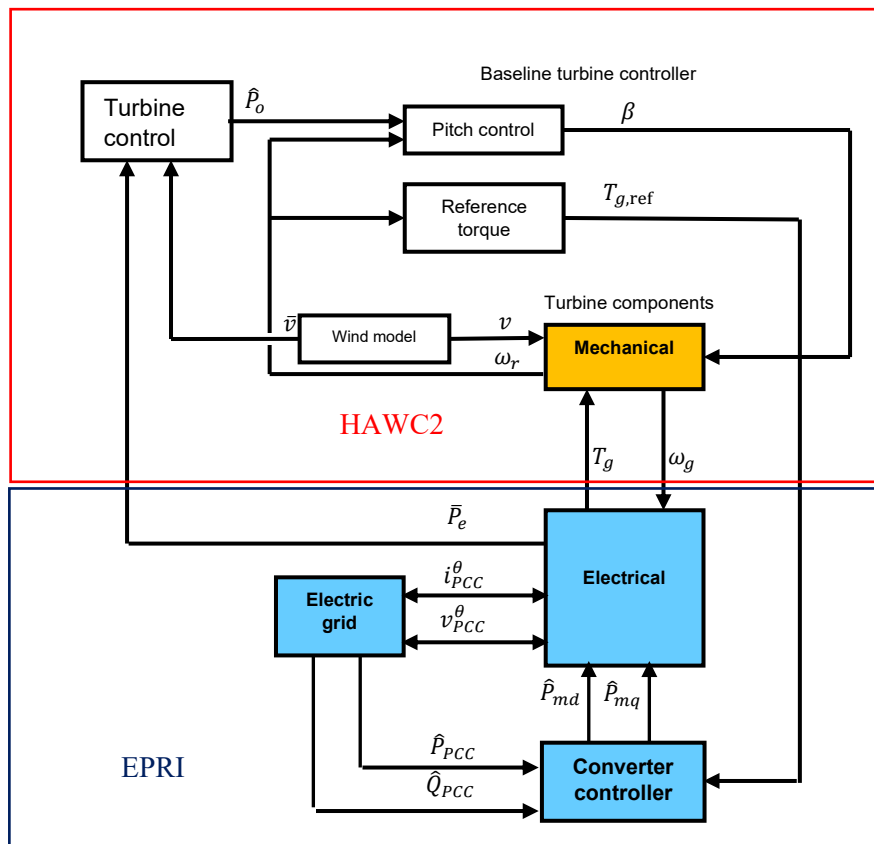


Figure 8 Integrated Mechanical and Electrical Framework

6.1. Electrical model components

After a thorough assessment of Teesside wind farm, the SWT-2.3-93 turbine has been identified to be part of the type IV classification:

- The NetConverter® system is a full rated power back-to-back converter and the only path of the generator to transmit power to the grid.
- The vendor guarantees that all hardware and control features necessary to satisfy the applicable GC's grid disturbance requirements are present.
- The generator is a squirrel cage induction. Although, its main characteristics and steady state values are well defined in the technical datasheet, no data has been provided for dynamic analysis. However, an equivalent synchronous machine model has been provided for transient analysis.
- The electric Grid is composed by two feeders in a semi-ring shape layout where all WTGs in the wind farm can be connected to the grid by closing the circuit breaker at the substation.

The details of the modelling approach of each of these modules will be explained in the following subsections.

6.2. Generator

The Generator model has been implemented using the “Park model representation” with the rotor-oriented dq (direct-quadrature) frame of the rotor [14]. This model can be described by the following equations in per unit (p.u.) system:

$$\dot{x} = A * x + u * \omega \quad (1)$$

Where:

$$x = \begin{bmatrix} \psi_q \\ \psi_d \\ \psi_{fd} \\ \psi_{kd} \\ \psi_{kq} \end{bmatrix}$$

$$u = \begin{bmatrix} e_q \\ e_d \\ Vf \\ 0 \\ 0 \end{bmatrix}$$

ψ_q : Stator winding flux (q axis)
 ψ_d : Stator flux winding (d axis)
 ψ_{fd} : Rotor winding flux
 ψ_{kd} : Damper winding flux (d axis)
 ψ_{kq} : Damper winding flux (q axis)
 e_q : Stator voltage (q axis)
 e_d : Stator voltage (d axis)
 Vf : Excitation voltage

$$A = -(R * L^{-1} + W);$$

A: State space Matrix

Composed by:

$$L = \begin{bmatrix} xaq + xl & 0 & 0 & 0 & xaq \\ 0 & xad + xl & xad & xad & 0 \\ 0 & xad & xffd & xfld & 0 \\ 0 & xad & xfld & x11d & 0 \\ xaq & 0 & 0 & 0 & x11q \end{bmatrix};$$

xaq : Mutual reactance (d axis)
 xad : Mutual reactance (q axis)
 xl : Stator leakage reactance
 xfd : Excitation winding reactance (d axis)
 $x1d$: Damper winding reactance (d axis)
 $x1q$: Damper winding reactance (q axis)
 $xrld$: Coupling reactance field and damper (d axis)
 $xffd$: $xad + xrld + xfd$
 $xfld$: $xad + xrld$
 $x11d$: $xad + xrld + x1d$
 $x11q$: $xaq + xrlq + x1q$

$$R = \begin{bmatrix} rstr & 0 & 0 & 0 & 0 \\ 0 & rstr & 0 & 0 & 0 \\ 0 & 0 & rfd & 0 & 0 \\ 0 & 0 & 0 & r1d & 0 \\ 0 & 0 & 0 & 0 & r1q \end{bmatrix};$$

$rstr$: Stator winding resistance
 rfd : Excitation winding resistance
 $r1d$: Damper winding resistance (d axis)
 $r1q$: Damper winding resistance (q axis)

$$W = \begin{bmatrix} 0 & \omega & 0 & 0 & 0 \\ -\omega & 0 & 0 & 0 & 0 \\ 0 & 0 & 0 & 0 & 0 \\ 0 & 0 & 0 & 0 & 0 \\ 0 & 0 & 0 & 0 & 0 \end{bmatrix};$$

ω : Rotor speed

This model considers stator windings, damper windings in dq axis and excitation windings in d axis. The inductances associated with damper windings can either represent real windings or eddy currents in the rotor. Hence the model can represent a generator with or without damper windings. In case of use of Automatic Voltage Regulators (AVR), this can be considered by connecting the controller output to V_f . If permanent magnets are considered then, it is only necessary to consider the excitation current constant i_{fd} in equation ((2).

$$i_{fd} = (V_f - \psi_{fd})/rfd \quad (2)$$

Where:

i_{fd} : Winding field current
 V_f : Excitation voltage
 ψ_{fd} : Excitation winding flux variation
 r_{fd} : field winding resistance

For this implementation an AVR has been included in the model. The main objective here is to maintain excitation flux constant. This is attained by PI block that calculates the required excitation voltage for a given flux error. In case of rotor speeds > 1 , the reference flux is decreased inversely proportional to the speed as show in Figure 9.

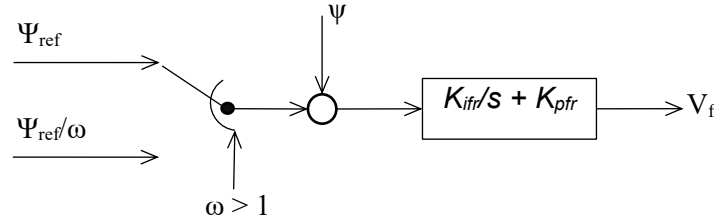


Figure 9 Synchronous generator excitation control

Where:

ψ : flux estimation feedback
 ψ_{ref} : flux reference
 V_f : Excitation voltage
 ω : Rotor speed
 K_{ifr} : Integral gain for voltage regulation
 K_{pfr} : Proportional gain for voltage regulation

According to Teesside WTG general description in chapter 5, equation (1) has been used to calculate the parameters for the synchronous equivalent generator in Appendix A.

The generator air-gap torque or commonly called the electric torque, is calculated based on the stator fluxes and the stator currents based on the d-q reference frame provided by the rotor, as shown by equation (3).

$$T_e = \psi_d * i_q - \psi_q * i_d \quad (3)$$

Where:

ψ_d : Stator flux d axis
 ψ_q : Stator flux q axis
 i_d : Stator current d axis
 i_q : Stator current q axis

During normal operation, a common practice in industry is to control the torque through the stator current i_q as an increment of it will provide a proportional increment in the torque. However, the fluxes are subject to changes caused by the stator voltages or the rotor speed. To mitigate this, a PI torque controller is added to the desired i_q stator current reference. This controller will be explained in detail in the following section (see Figure 11).

6.3. Back-to-Back converter

The back-to-back converter is modeled as two self-commutated inverters with IGBTs which is the common practice in industry when synchronous generators with excitation or permanent magnets are used. These are named Generator-side and Grid-side converters respectively.

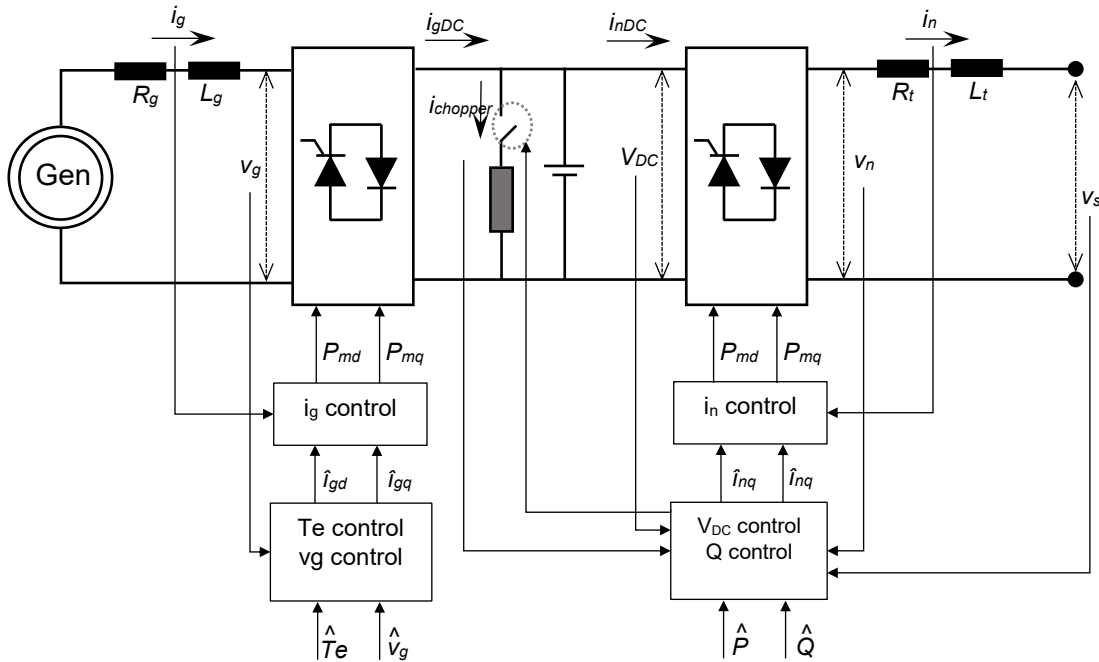


Figure 10 Back-to-back Converter & Control System

Where:

i_g : Generator side converter current
 i_{gDC} : Generator side DC link current
 i_{nDC} : Grid side DC link current
 i_n : Grid side converter current
 $i_{chopper}$: Chopper current
 v_g : Generator side converter voltage
 v_n : Grid side converter voltage
 V_{DC} : DC link converter voltage
 P_{md} : Modulation index d axis

P_{mq} : Modulation index q axis
 i_{gd} : Generator side current reference d axis
 i_{gq} : Generator side current reference q axis
 i_{nd} : Grid side current reference d axis
 i_{nq} : Grid side current reference q axis
 \hat{P} : Power generation reference
 \hat{Q} : Reactive power generation reference
 \hat{T}_e : Torque reference
 \hat{v}_g : Generator voltage reference

The Generator side converter controls the AC Voltage at the stator. This is particularly important for synchronous generators.

Depending on the wind speed conditions, the turbine controller sends a torque reference. This is received by the Generator-side and later translated to a current set point by a PI block as show in Figure 11.

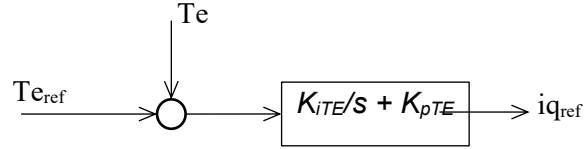


Figure 11 **Electric Torque PI controller.** This controller tries to minimize any perturbations in the torque caused by oscillation of the stator fluxes. This is achieved by continuously adjusting the current reference signal.

Where:

T_{ref} : Torque reference

T_e : Torque feedback

i_{qref} : Current reference q axis

K_{ifr} : Integral gain for voltage regulation

K_{pfr} : Proportional gain for voltage regulation

The Generator-side has been provided with a fast loop with dead band that controls the DC voltage during LVRT events. This additional loop is activated when the DC-voltage surpasses a high threshold in which case it decreases the i_q setpoint to reduce the torque. The purpose of the dead-band is to avoid unnecessary reactions of this loop during normal operation where the Grid-side converter controls the DC-voltage continuously.

During a voltage sags, the DC-voltage can increase rapidly. In such cases, a chopper connected in parallel limits the voltage rises to 1.1 p.u. to avoid any damage in the DC capacitors. Although the chopper action is crucial during a fault, the fast action of the Generator-side converter decreases the power production and reduces the amount of energy to be burned by the chopper. These controllers are depicted in Figure 12.

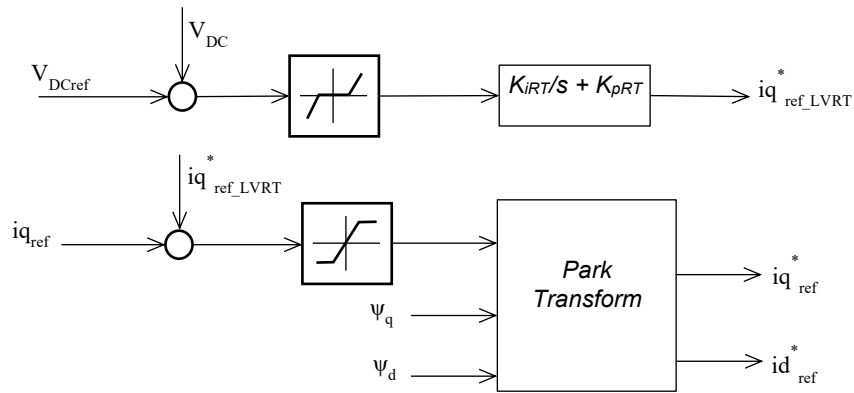


Figure 12 **Generator side outer loop control.** The controller receives the current set point to produce a desired torque. A LVRT current reference is added to perform fast corrections in case of LVRT events. Finally a Park transformation is performed in the current signals to align the controller with the rotor frame or reference.

Where:

V_{DC} : DC voltage feedback

V_{DCref} : DC voltage reference

$i_{qref_LVRT}^*$: Current reference q axis LVRT fast action

i_{qref} : Current reference q axis from torque controller

i_{qREF}^* : Current reference q axis in rotor flux oriented frame

i_{dREF}^* : Current reference d axis in rotor flux oriented frame

ψ_d : rotor flux in d axis

ψ_q : rotor flux in a axis

K_{iRT} : LVRT fast control integral gain

K_{pRT} : LVRT fast control proportional gain

These outer loops provide the current references to a faster inner current loop which is the common practice in industry. These inner loops are composed by a PI block which outputs gives the modulation index signal to the PWM switching module. This can be observed in detail in Figure 13

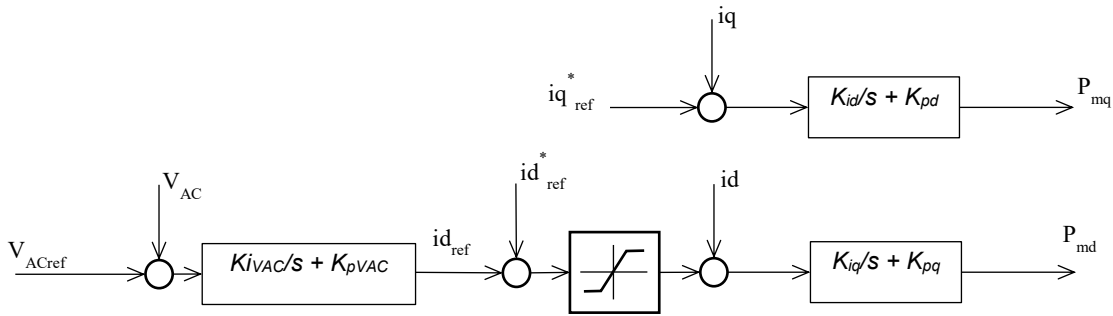


Figure 13 Generator side current control.

Where:

- V_{AC} : Stator voltage feedback
- V_{ACref} : Stator voltage reference
- iq_{ref}^* : Current reference q axis in rotor flux oriented frame
- iq : Current feedback q axis
- id_{REF}^* : Current reference d axis
- id : Current feedback in rotor flux oriented frame
- K_{iVAC} : integral gain stator voltage control
- K_{pAC} : proportional gain stator voltage control
- K_{id} : integral gain current control
- K_{pq} : proportional gain current control

If the WTG produces more power, the DC-link increases due to a surplus of current. This will be measured by the Grid-side converter and will react by increasing power transfer to maintain the DC-voltage on a constant level.

The reactive power (Q_{grid}) transmitted to the grid is also controlled to comply with GC standards. In case of voltage deep, a LVRT signal might be activated which will switch the power production priority to cope with the grid support requirements (and by this shutting down the active power generation). Similarly, to the Generator-side converter, these controllers produce a current reference to a faster inner current controller which give the modulation index to the PWM module. The Grid-side converter controllers are depicted in Figure 14.

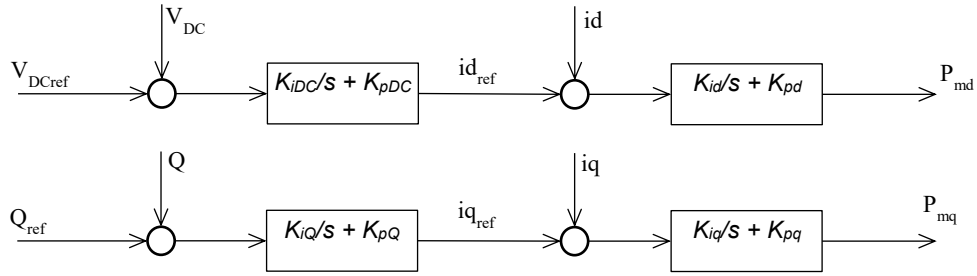


Figure 14 **Grid side outer and current controls.** DC voltage is controlled by the d channel or active power channel and reactive power is controlled by the q channel or reactive power channel. To achieve this, the grid side controller is synchronized with the q axis of the measured voltage at PCC.

Where:

V_{DC} : DC link voltage feedback
 V_{DCref} : DC link voltage reference
 i_{qref} : Current reference q axis
 i_q : Current feedback q axis
 i_{dref} : Current reference d axis
 i_d : Current feedback
 K_{IDC} : integral gain DC voltage control
 K_{pDC} : proportional gain DC voltage control
 K_{id} : integral gain current control
 K_{pq} : proportional gain current control

The DC link is composed by the chopper and the DC capacitor. The capacitor provides a stable DC voltage for both converters, which can be calculated by equation (4)

$$\dot{V}_{dc} = \frac{i_{Gen} - i_{Grid} - i_{Chopper}}{C_{dc}} \quad (4)$$

Where:

\dot{V}_{dc} : DC link voltage deviation
 i_{gen} : genertor side dc current
 i_{grid} : grid side dc current
 $i_{chopper}$: chopper current
 C_{dc} : DC link capacitor

The Chopper main task is to prevent the DC voltage to rise to an unsecure level for the DC capacitor. In this sense, when DC voltage rises over 1.1 p.u., the chopper buck-boost converter will start switching the gates so the energy excess will be dissipated by a resistor. The operation is stopped if the voltage decreases below 1.09 p.u.

6.4. Electric Grid

The electric system between the wind farm and the power grid is composed by a set of feeders which are electric cables that transmit the power generated by the WTG. In general, these electrical components can be modeled by currents through impedances with defined voltages at both ends. The relationship of these extreme voltages defines the power transfer between the source and the grid. A single line representation of a balanced 3-phase system can be observed in the following Figure 15.

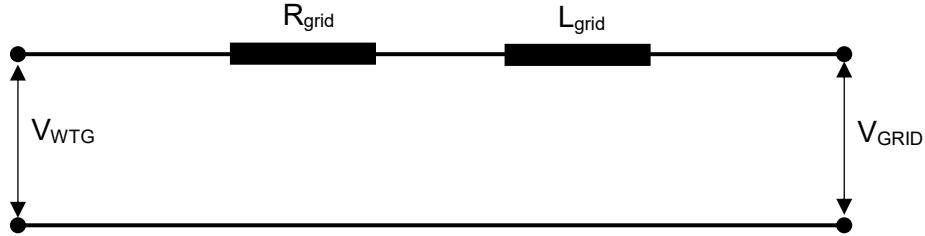


Figure 15 Simplified Electric Grid model.

The equations describing “a” phase of the cable is shown in equation (5)

$$V_{a\ WTG} = i_a * R_{grid} + L_{grid} \frac{di_a}{dt} + V_{grid} \quad (5)$$

Where:

$V_{a\ WTG}$: Phase a voltage at WTG busbar
 V_{grid} : Phase a voltage at equivalent external grid busbar
 i_a : Phase a current
 R_{grid} : condensed grid resistance
 L_{grid} : condensed grid inductance

The dq representation after the Park transformation of the complete positive sequence system is show in equation (6) [15]:

$$\begin{bmatrix} \hat{i}_d \\ \hat{i}_q \end{bmatrix} = \begin{bmatrix} -\frac{R_{grid}}{L_{grid}} & \omega \\ -\omega & -\frac{R_{grid}}{L_{grid}} \end{bmatrix} * \begin{bmatrix} i_d \\ i_q \end{bmatrix} + \begin{bmatrix} \frac{1}{L_{grid}} & 0 \\ 0 & \frac{1}{L_{grid}} \end{bmatrix} * \begin{bmatrix} V_{d\ WTG} - V_{d\ grid} \\ V_{q\ WTG} - V_{q\ grid} \end{bmatrix} \quad (6)$$

Where:

$V_{d/q\ WTG}$: voltage at WTG busbar in d/q axis
 $V_{d/q\ grid}$: voltage at equivalent external grid busbar in d/q axis
 $i_{d/q}$: Phase a current in d/q axis
 R_{grid} : condensed grid resistance
 L_{grid} : condensed grid inductance

In this representation, the inverter's reactor and the transformer have been included in the total grid impedance. However, the measurements used for the controller are usually taken from the transformer HV side. To account for this the obtained state variables i_d and i_q are retrofitted to calculate the transformer voltage with the following equations (7) and (8).

$$V_{d\ trafo} = i_d * \frac{(R_{Line}L_{trafo} + L_{Line}R_{trafo})}{L_{grid}} + (V_{d\ grid} - V_{d\ WTG}) * \frac{L_{trafo}}{L_{grid}} + V_{d\ WTG} \quad (7)$$

$$V_{q\ trafo} = i_q * \frac{(R_{Line}L_{trafo} - L_{Line}R_{trafo})}{L_{grid}} + (V_{q\ grid} - V_{q\ WTG}) * \frac{L_{trafo}}{L_{grid}} + V_{q\ WTG} \quad (8)$$

6.5. Mechanical model components

The Simulink based EPRI's electrical model is coupled with DTU aeroelastic tool HAWC2 [16] through the TCP/IP protocol as shown in Figure 16 and previous developed by [17] and [18]. In this coupling framework, MATLAB starts HAWC2 and then these two models interact with each other in an orderly fashion. This means that there is exchange of information at every time step, hence this framework is a fully coupled approach. The previous implementations of a Simulink model of the drive train combined with a HAWC2 model has addressed the radial load mitigation through gearboxes coupled with a Double Fed Induction Generator (DFIG) in the Type 3 drive train configuration where the stator windings are coupled directly to the electrical grid [18] and [19]. In this study a squirrel cage generator is coupled fully through a power converter in a drive train of Type 4 and the focus is to determine the main bearing loads, since this is an expensive component (€200,000 - €250,000) to replace in the drive train. The reason for the high cost of replacement is that one will have to unmount the turbine rotor from the main shaft, before the main bearing can be replaced and then the turbine rotor must be remounted. This demand the availability of a jack-up vessel with a large crane for performing the operation. One can in general say that a similar jack-up vessel is needed to replace a full gearbox from offshore wind turbine, whereby full gearbox replacements are as expensive as the main bearing replacement, but often some minor gearbox failures can be repaired up-tower without removing the gearbox from the nacelle. The current electrical model is targeting to describe the power converter and the implementation of the Low Voltage Ride Through control.

The detailed description of the HAWC2 aeroelastic model of the Siemens SWT-2.3-93 [12] is given in the HIPEWIND deliverable D5.1. The HAWC2 aeroelastic tools computes the aeroelastic loads and responses of mechanical components of a wind turbine in time domain. The DTU wind energy controller [20] is employed in HAWC2 by means of Dynamic Link Libraries (DLLs) for controlling the wind turbine. It uses generator torque control strategy for below rated wind speeds (rated mean wind speed for Siemens SWT-2.3-93 [12] is 12 m/s) and the pitch control strategy for above rated wind speeds. More details about the HAWC2 control algorithm can be found in [20]. The HAWC2 aeroelastic tool computes the reference torque ($T_{g,ref}$) together with aeroelastic loads at the beginning of the simulation. The computed $T_{g,ref}$ is sent to the Simulink electric model through TCP/IP protocol. Based on the $T_{g,ref}$ and the grid situation, the electrical generator torque (T_e) is computed and sent back to HAWC2 in the same time step. Finally, the received T_e will be used to compute $T_{g,ref}$ for the next time step in HAWC2 and this loop goes on until the simulation ends. The influence of the grid faults on the drivetrain main bearing is the focus here. The Siemens SWT-2.3-93 [12] main shaft is supported by single spherical roller bearing and its definitions are given in the HIPEWIND deliverable D5.1.

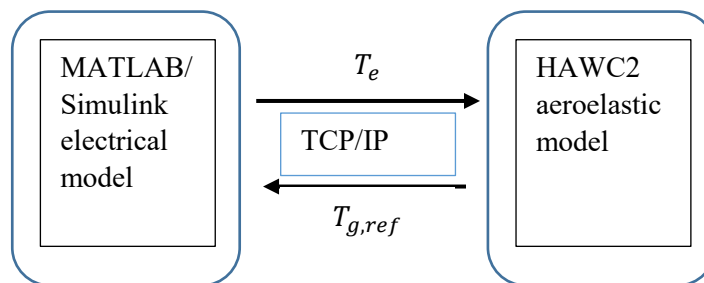


Figure 16: TCP/IP based coupling of the electrical model with the HAWC model of the SWT 2.3 – 93 turbine.

7. LVRT Time domain Simulations

As previously mentioned in chapter 4.1, 3-phase to ground faults only constitutes less than 10% of all events. However, WTG converters possess current controllers that are capable of suppressing currents in negative or zero sequences even when the fault is unbalanced. With this feature, the current been fed to the fault will be of positive sequence and only under some specific circumstances negative current could be injected (some GCs will require negative current injection to mitigate the voltage unbalance). This means that unbalanced and balanced faults will trigger the same kind of response from the inverter, and both will be perceived as balanced faults by the control system in general terms. To show case this, the following test system has been prepared where a single WTG is connected to an infinite bus (see Figure 17)

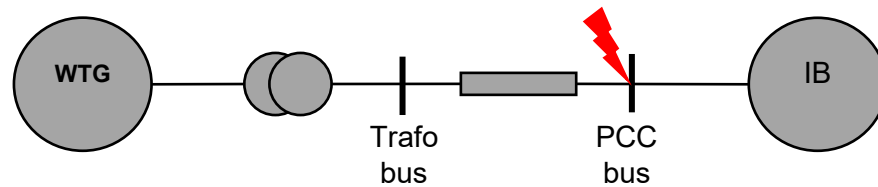


Figure 17 Wind turbine generator connected to an Infinite Bus. A short circuit event takes place at the Point of Common coupling between the grid and the Wind Turbine Generator

To test the system response under different grid disturbances, two faults (3-phase SC and 1-phase to ground SC) are applied at the Point of Common Coupling (PCC) and the 3-phase voltages are measured. The fault duration is set to last for 200 ms in both cases and cleared after. The resulting voltages at the PCC and the transformer can be observed in Figure 18.

In case of the 3-phase fault, all 3 phases drop to 0 at the PCC due to the applied SC without impedance, however, the transformer still shows a residual voltage due to the grid impedance. In case of the 1-phase to ground fault, only the faulted phase drops to 0 whereas the rest still shows normal rated voltage. Similarly, the transformer bus will still show residual voltage due to the grid impedance.

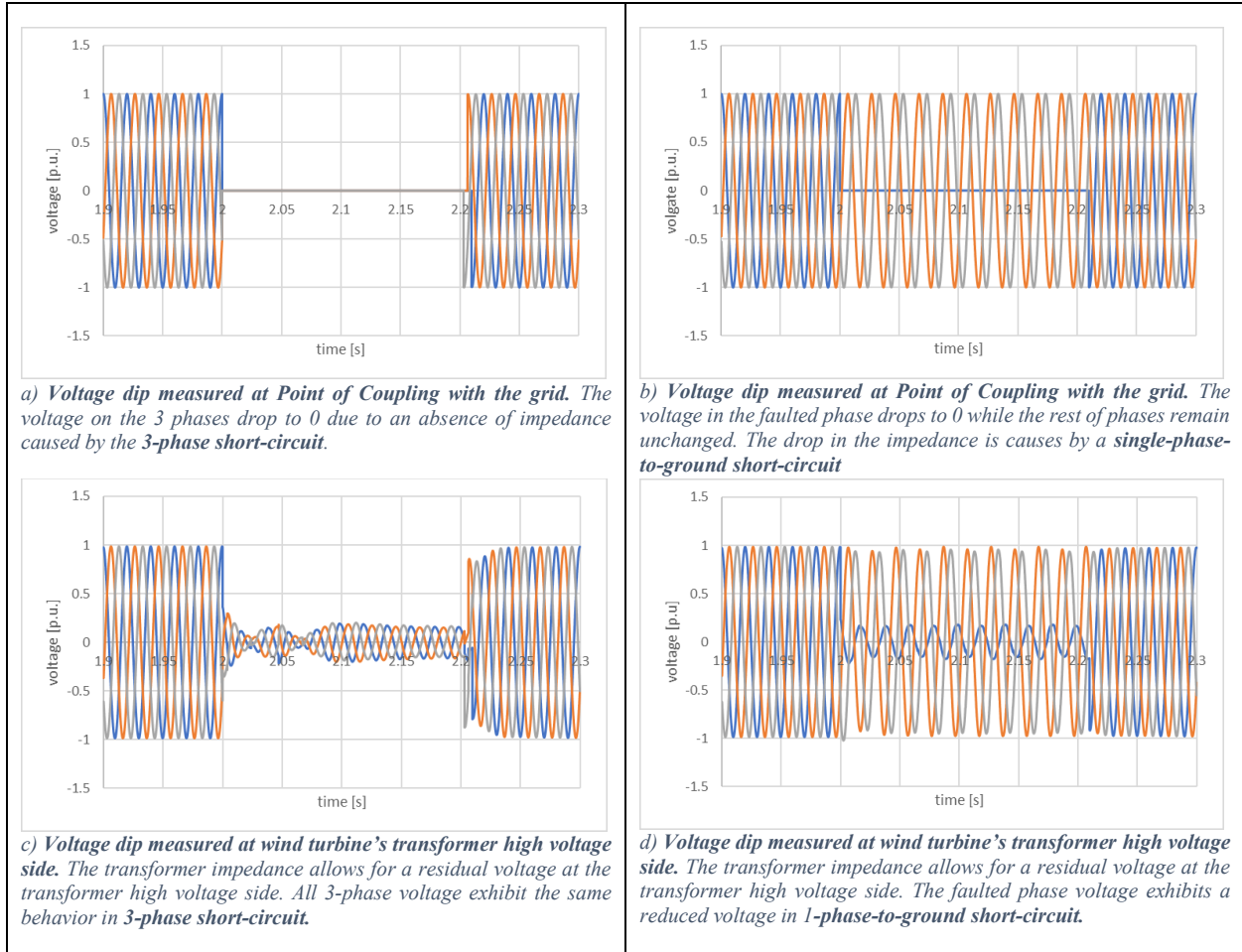


Figure 18 3-phase Short Circuit vs 1-phase to ground. 3-phase voltage behavior

In Figure 19 the power produced by the WTG has been measured for both cases. In case of the 3-phase fault, the active power drops to 0 for the duration of the fault and requires more time to recover after the fault has been cleared. For the 1-phase fault, active power is transferred through the healthy phases even during the fault. As previously stated, for the control system this can be viewed as a less severe fault where power can be transferred even during the duration of the fault.

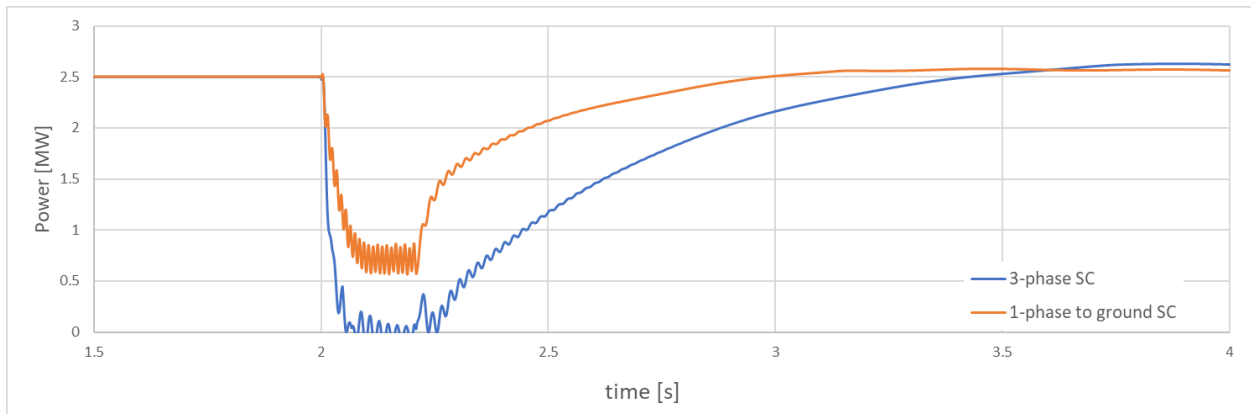


Figure 19 Active power generation during Grid voltage sag at 12m/s wind speed. The response has been simulated using an IEC-2.5MW type 4 wind turbine model in powerFactory.

As the main objective of this study is to assess the impact of the LVRT over the structure, a worst-case scenario has been designed for that purpose which will constitute the baseline of the study. Assuming that any other case will be less aggressive to the structure, it could be possible to measure what could be the highest damage if the most harmful scenario is repeatedly observed.

This consists of applying a 3-phase short circuit fault at the PCC of the WTG. The deep and duration of the fault has been tuned to coincide with the maximum requirements of the GCs with the highest demand belonging to the Chinese and US GCs. This means that the fault will be as deep and long as possible but without producing a disconnection as mandated by design load cases which are covered in later chapters.

When the short circuit is applied, it is assumed that the fault has no impedance to ground. To simulate this, the grid has been model as an infinite power source connected at the PCC for the duration of the fault. This means that the voltage level at the PCC will absorb any amount of current without varying its voltage. The following Figure 20 shows the behavior of the voltage magnitude in p.u. during a fault at the PCC and the measured voltage magnitude at the connection transformer.

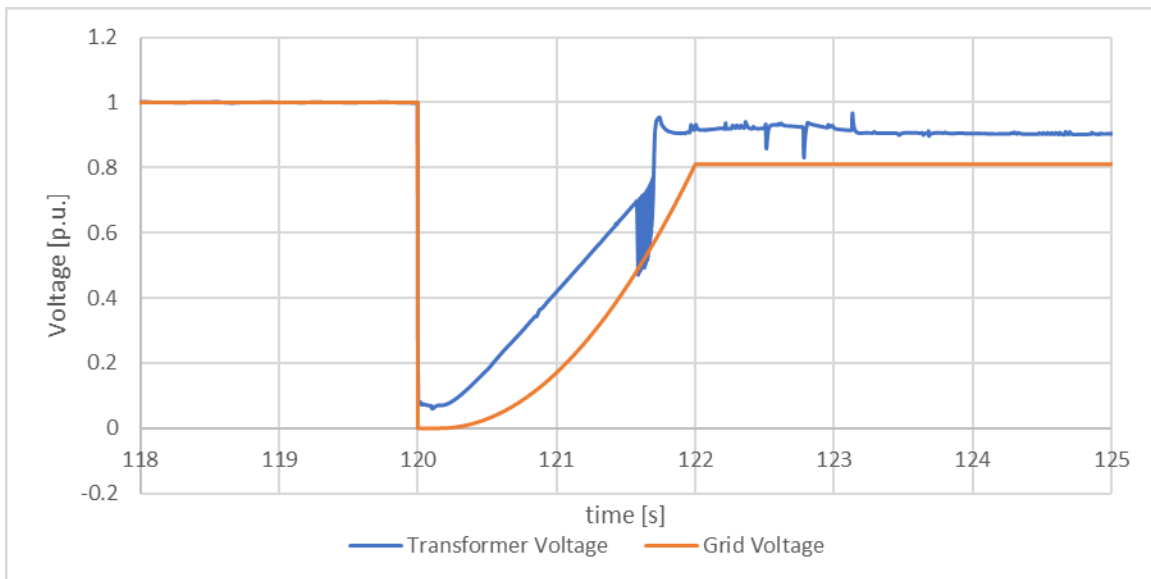


Figure 20 Voltage sag profile with a duration of 2s at Transformer (blue) and PCC (orange). The observed voltages at PCC and at high voltage side of the wind turbine transformer are slightly different due to the transformer impedance as expected.

During the fault, the Grid-side converter is not able to transfer power to the grid, as a consequence, the DC-link voltages increase rapidly. In Figure 21 the same fault has been simulated with and without the LVRT controller added in the Generator-side controller.

The fault is trigger at 120s. When the LVRT controller is active, it can be observed that the chopper is activated only for a fraction on the fault duration and chopper's current is dissipated through the resistor only for a few moments. Although, the DC voltage manage to stay below 1.1 p.u. during the complete sequence. In the opposite case without the controller, the chopper sustains operation during the complete fault duration and the DC voltage remains closer to 1.1 p.u..

Finally, the total dissipated energy by the chopper in both cases is compared. The dissipated energy with LVRT controller active is just a small fraction of that one without the controller. This in principle implies a more secure operation for the DC capacitor and further, the chopper resistor could decrease in size due to a less demanding operation.

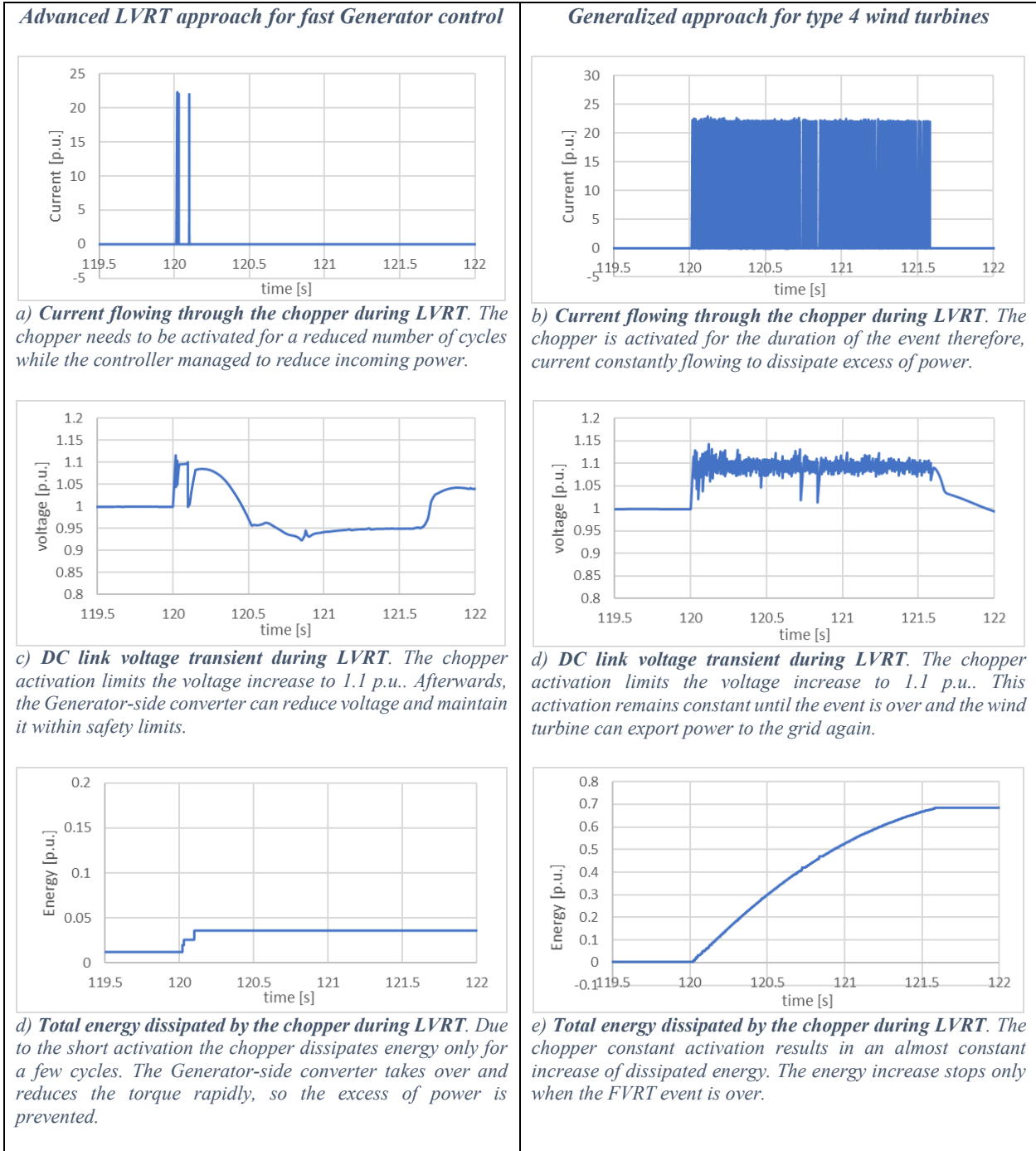


Figure 21 Differences in chopper energy dissipation with dedicated Generator side LVRT-controller. With the fast LVRT-controller (left-hand charts) the chopper activation is much shorter resulting in less energy dissipation. In contrast, with the generalized approach (right-hand side charts) the chopper remains active for the duration of the fault resulting in a much higher energy dissipation

The generator torque shows a different behavior during the fault due to Generator-side converter as well. In Figure 22 this shown for both cases, with and without controller. With the LVRT controller, the generator current is reduced given as a result a reduction in the torque as well. In the case without the controller, the generator torque exhibits only small perturbations of high frequency, but the overall behavior does not diverge much from normal behavior.

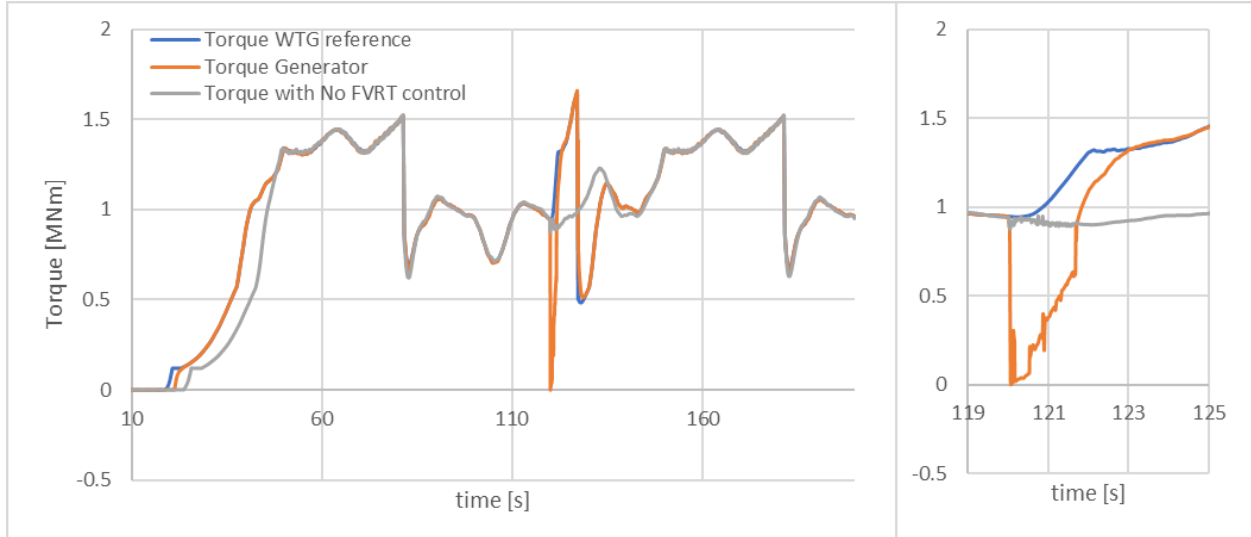


Figure 22 **Torque reference and actual generated torque for a wind speed of 12 m/s with turbulence.** The figure depicts two operation scenarios, one with LVRT event (orange/blue signals) and one without events (gray). In the case with LVRT it can be observed the immediate drop of torque (120s) from the generator (orange) and later the turbine control reaction (blue) that will produce an overshoot after the event is past. In case of no events, the generator torque follows the wind turbulence profile.

As a result of the fast drop in generator torque due to the LVRT controller, the generator speed is affected as well. During the fault, wind speed and blade pitch are maintained roughly the same and therefore, the mechanical torque is not modified. In normal operation, mechanical and generator torque are equalized except for the losses in the drivetrain. The sudden change in generator torque produces an imbalance in this relation giving as a result an acceleration of the rotor. This last is shown in Figure 23.

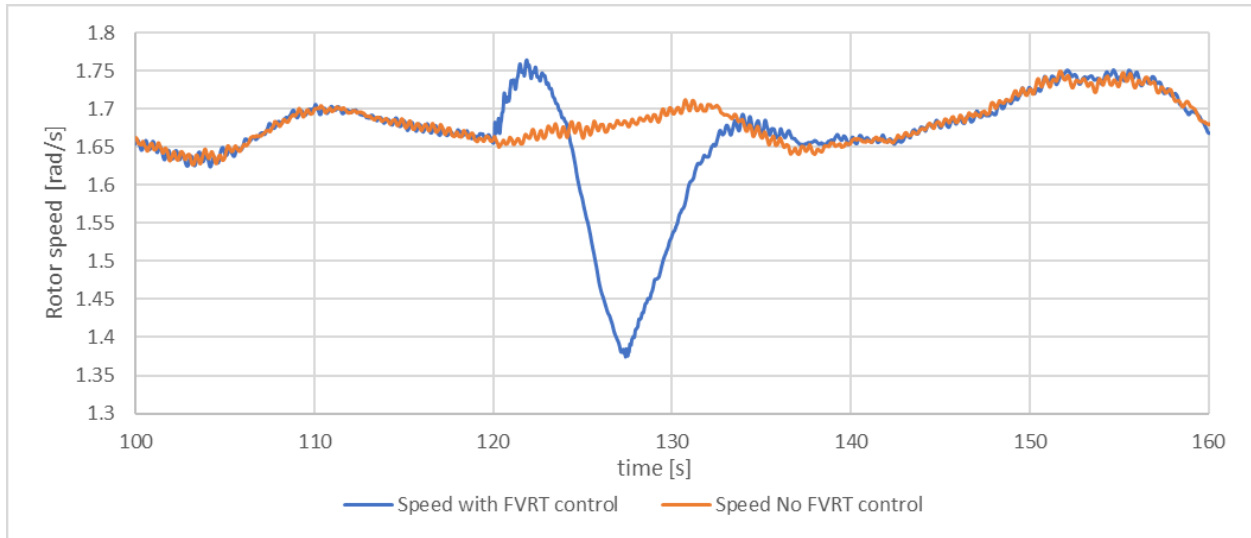


Figure 23 **Generator speed acceleration for a wind speed of 12 m/s with turbulence.** In case of LVRT event (blue signal), the rotor speed experience a sudden acceleration due to the drop in torque continued by a steady increase caused by the turbine control reaction until the nominal speed is reached back. In case of no events, the rotor speed continues to oscillate around nominal speed (orange signal).

8. Results

The influence of the grid faults on the main bearing loads will be discussed here through the developed electro-mechanical model presented in Section 5. The electro-mechanical simulations are performed for IEC [21] specified design load cases (DLCs) for grid faults during wind turbine operation. There are two such DLCs: (i) DLC 2.4 is for the fatigue load assessment, and (ii) DLC 2.5 is for the ultimate load assessment. From these two load cases, the main bearing loads are computed using the electro-mechanical model and the results of these two load cases will be discussed here in detail.

8.1. DLC 2.4 Power production with loss of electrical network

The description of the DLC 2.4 as per IEC standard [21] is given in Table 3. It consists of six turbulent seed simulations for each mean wind speed resulting in a total number of 72 simulations under DLC 2.4. The Siemens SWT-2.3-93 [12] is certified for IEC wind class II A that corresponds to the reference turbulence intensity (I_{ref}) of 0.16 and the annual mean wind speed (V_{ave}) of 8.5 m/s.

Table 3: Description of the DLC 2.4.

Load case	DLC 2.4
Design situation	Normal power production with grid fault
Mean wind speed at hub height (V_h)	4-26 m/s in step of 2 m/s
Turbulence model	Normal turbulence model (NTM) (6 seeds)
Wind yaw	0 [deg]
Wind shear	0.14
Waves	Normal sea state (NSS), $H_s = E[H_s V_h]$, Here, H_s – Significant wave height, T_s - wave time period. (See Deliverable 5.1 for details).
Wind and wave directionality	Uni-directional
Wave yaw	0 [deg]
Sea currents	No currents
Simulation time and sampling frequency	100 s (Without 100 s transients) and 100 Hz
Grid loss through FVRT initiation time	$t = 20$ s

The LVRT event is triggered at $t = 20$ s for all the 72 simulations. Figure 24 (a) is showing the wind speed time series with a turbulence intensity of $I_{ref} = 0.16$ and different average wind speeds used in the HAWC2 simulations. The resulting generator torque (T_g), the turbine rotor rotation speed and the corresponding blade pitch angle (β) are shown in Figure 24 (b), (c) and (d) respectively. As seen in Figure 24 (b) the generator torque comes to zero around $t = 20$ s and ramp -up to its desired value at the end of FVRT action which typically lasts for 1-3 s. As a result of T_g going to zero, the controller is reacting by adjusting the blade pitch angle according to T_g value for the above rated mean wind speeds as in Figure 24 (d). For below rated mean wind speed ($V_h < 12$ m/s), since the pitch control is not active the blade pitch angle is kept at a

constant value as seen in Figure 24 (d). It should be noticed that the LVRT control scheme as illustrated in Figure 8 is using the philosophy of interacting with the power converter control of drive train by activating the chopper to keep the voltage on the DC capacitor of the converter limited as the grid is lost while decreasing the generator current and thereby the electromagnetic torque of the generator as illustrated in Figure 21 to limit the heating of the chopper resistor. Thus, the pitch controller of the turbine is not changed in the current implementation of the LVRT control. By looking in Figure 24 (d) it can be seen that the pitch controller of the turbine is getting somewhat confused about the LVRT event and since the pitch controller is used to keep a constant power production of the turbine output then the pitch angle is actually lowered in order to increase the power production, because the pitch controller is detecting that the output power has decreased to zero. About 5 seconds later, the turbine rotor speed is peaking, and the pitch controller starts to increase the pitch angle towards the normal operation, which is obtained about 10 seconds after the LVRT as shown in Figure 24 (c). Thus, the pitch controller is actually amplifying the effects of the LVRT but is delayed peaking several seconds after the LVRT event is over from a grid side point of view. This means that one could improve the LVRT control even further if the pitch controller was also controlled during the LVRT, but it will be examined in this report if it is needed in the context of the main bearing.

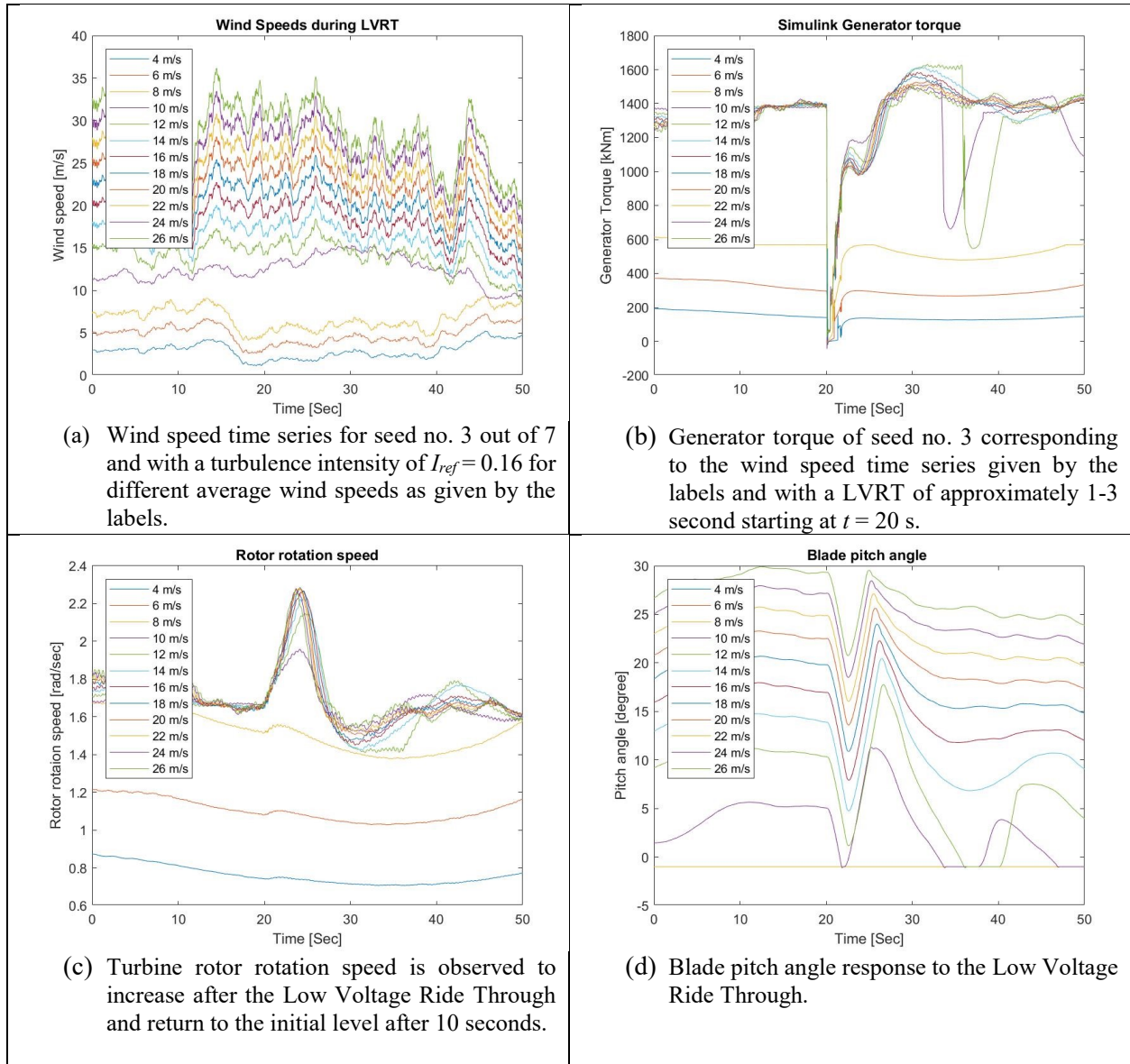


Figure 24 HAWC2 response time series during Low Voltage Ride Through (LVRT) at $t = 20$ seconds under DLC 2.4 with a turbulence intensity of $I_{ref} = 0.16$. Only 50 seconds out of 100 seconds are shown to highlight the features after the LVRT, whereas all 100 second time series are used for the fatigue evaluation.

The main bearing loads are obtained in all three directions (*i.e.*, axial (F_a), lateral (F_x) and vertical (F_y)) from these 72 electro-mechanical simulations. All loads are in the bearing rotational coordinate system and then the main bearing radial load is obtained as $F_r = \sqrt{F_x^2 + F_y^2}$. Finally, the resultant damage equivalent fatigue load, DEFL (P_d) is obtained by combining the radial and axial loads using the Load duration distribution method [22] for each simulation. The resultant mean values of F_r , F_a and P_d as a function of mean wind speed under DLC 2.4 is shown in Figure 25. As seen in the figure, the radial load does not undergo much variation with respect to the mean wind speed. Whereas the axial load and the DEFL

increases till the rated mean wind speed and then starts decreasing with an increase in the mean wind speed. This is because of the strong correlation between the main bearing axial load and the rotor thrust. In addition, the similar behavior between the axial load and the DEFL shows that the DEFL is strongly dominated by the axial load response.

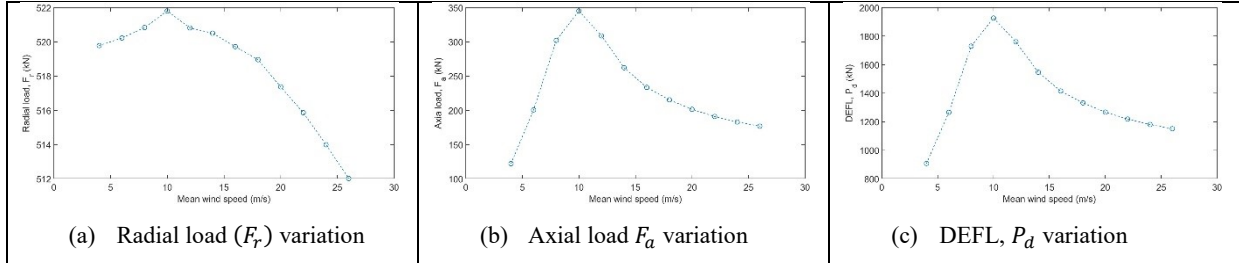


Figure 25: Main bearing loads as a function of mean wind speed for DLC 2.4 with $V_{ave} = 8.5$ m/s, and $I_{ref} = 0.16$.

Subsequently, the modified rating life (L_{nmh}) [23] for all these simulations can be computed as,

$$L_{nmh} = a_1 * a_{ISO} * \frac{1e6}{60 \omega} \left(\frac{C}{P_d} \right)^p \text{ [in hours]}, \quad (9)$$

where, C is the bearing-specific basic dynamic load rating, P_d is the damage equivalent fatigue load (DEFL), p is the bearing life exponent: $p = 10/3$ for roller bearings, ω is the angular speed of the bearing in rpm and the conversion factors are 60 min/h and $1e6$ (1 million) revolutions, a_1 is the life modification factor for reliability and, a_{ISO} is the life modification factor for special operating conditions such as lubrication conditions (*i.e.*, type and viscosity of the lubricant) and the contamination of the lubricants. When $a_1 = 1$, then L_{nmh} becomes L_{10mh} . This is a lifetime that will be survived by 90 % of bearings in an identical group.

The parameters in addition to P_d , that affect the bearing life are bearing operating temperature (T_B), lubricant viscosity (ν) and contamination level of the lubricant and these operational parameters are modelled in a_{ISO} . For the calculation of a_{ISO} the mean ambient temperature (T_A) is chosen as 22°C and the lubricant inside the main bearing is assumed to be in the normal cleanliness [23] level. The calculation procedure of a_{ISO} is detailed in the HIPEWIND deliverable D5.1. The resulting mean value variation of T_B , ν , the viscosity ratio ($\kappa = \nu/\nu_1$) and a_{ISO} are given in Figure 26. Here, ν_1 is the reference kinematic viscosity, which is a function of the bearing rotational speed (ω) and the pitch diameter. As seen in Figure 26(a), the main bearing temperature T_B exhibits a similar behavior as that of P_d with the mean wind speed, which indicates the direct correlation between them. As per temperature-viscosity relationship given in ASTM standard [24], the temperature and viscosity are inversely proportional to each other. As a result, the main bearing operating viscosity follows the inverted pattern of T_B with the mean wind speed as in Figure 26(b). From the Figure 26(c) and Figure 26(d), it is evident that κ and a_{ISO} are directly proportional to ν as they resemble the similar behavior with respect to the mean wind speed.

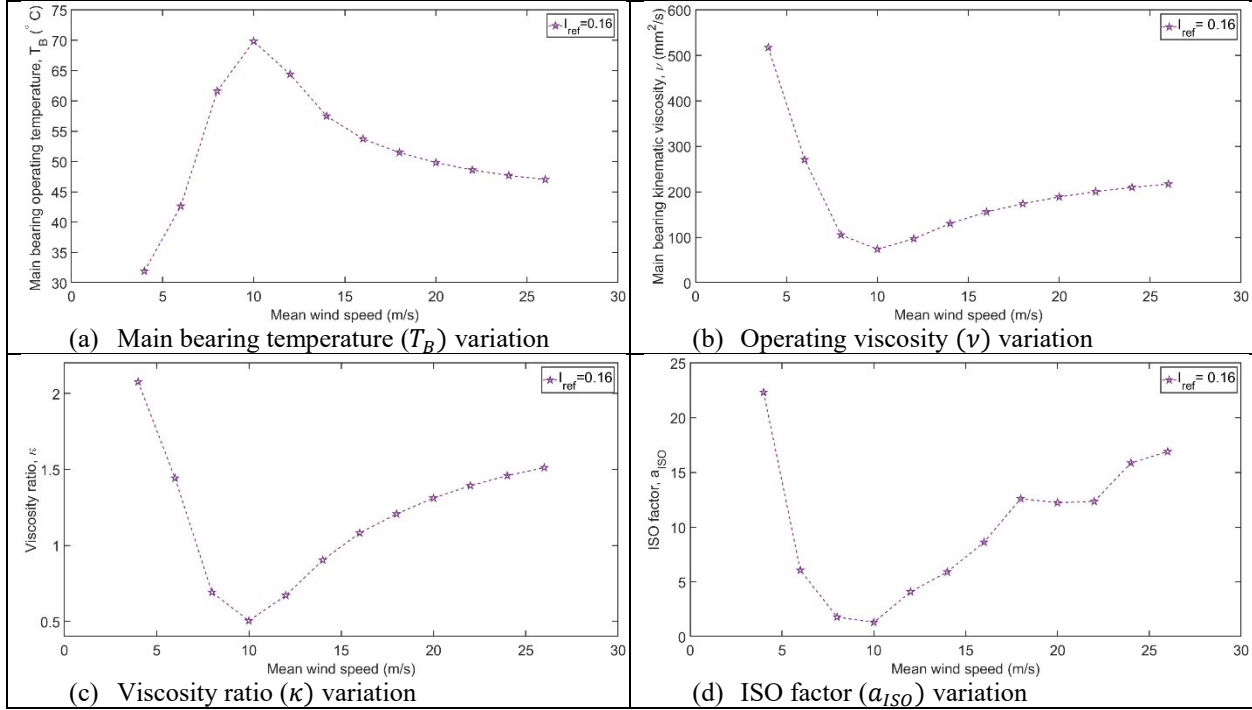


Figure 26: Variation of the main bearing operational parameters with mean wind speed (normal cleanliness, $T_A = 22^\circ \text{C}$).

After that, the equivalent life (L_{10mv}) for each mean wind speed (V_h) is obtained as,

$$L_{10mv}(V_h) = \sum_{i=1}^{N_1} \frac{L_{10h,i}}{N_1 * 365 * 24} \text{ [in years]}, \quad (10)$$

where, N_1 is the total number of ten min simulations for each mean wind speed under DLC 2.4 (i.e., $N_1 = 6$), and $L_{10h,i}$ is the modified rating life of i^{th} simulation.

The resulting modified life computed using Eq. (10) for each mean wind speed under DLC 2.4 are given in Figure 27 and it shows that the higher the a_{ISO} higher will be the life. Accordingly, the life is lowest for the mean wind speed of 10 m/s. If the wind turbine operates at a particular mean wind speed throughout the year, the resulting lifetime for that particular mean wind speed can be obtained from Figure 27.

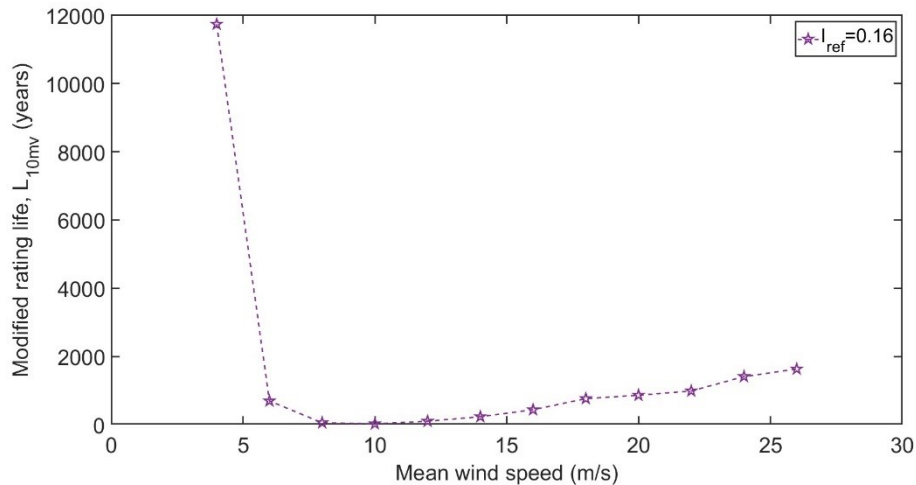


Figure 27: Variation of L_{10mv} with the mean wind speed under DLC 2.4

Finally, the total modified rating life L_{10mt} for DLC 2.4 can be obtained by combining the equivalent life (L_{10mv}) for each mean wind speed with its annual frequency occurrence ($P_R(V_h)$) as,

$$L_{10mt} = \frac{\sum_{j=1}^N P_R(V_{h,j})}{\sum_{j=1}^N \frac{P_R(V_{h,j})}{L_{10mv}(V_{h,j})}} \text{ [in years]}, \quad (11)$$

where, N is the total number of mean wind speeds under DLC 2.4 (i.e., $N = 12$), ($P_R(V_{h,j})$) is the annual frequency of occurrence of j^{th} mean wind speed given by Rayleigh distribution [21], and $L_{10mv}(V_{h,j})$ is the total modified rating life of j^{th} mean wind speed.

By combining individual life computed using Eq. (10) for each mean wind speed with its annual frequency of occurrence ($P_R(V_h)$), the resulting total fatigue lifetime of the main bearing is computed as $L_{10mt} = \mathbf{92}$ **years**. It means that if the wind turbine operates full under DLC 2.4 whereby the FVRT action takes places every 100s once then the resulting main bearing lifetime would turn out be 92 years. This shows that the high frequency FVRT action is not a concern for the main bearing fatigue life since the estimated fatigue lifetime is much higher than the design lifetime of 25 years.

8.2. DLC 2.5 Power production with Low Voltage Ride Through

The description of the DLC 2.5 as per IEC standard [21] is given in Table 4. A steady wind case and the wind profile at different heights can be modelled using normal wind profile (NWP) model given by the IEC standard [25]. A total of 12 simulations were conducted under DLC 2.5.

Table 4: Description of the DLC 2.5.

Load case	DLC 2.5
Design situation	Normal power production with grid fault
Mean wind speed at hub height (V_h)	4-26 m/s in step of 2 m/s
Turbulence	None
Wind profile	Normal wind profile (NWP)
Wind yaw	None
Wind shear	0.14
Waves	Normal sea state (NSS), $H_s = E[H_s V_h]$, Here, H_s – Significant wave height, T_s - wave time period.
Wind and wave directionality	Unidirectional waves
Wave yaw	None
Sea currents	No currents
Simulation time and sampling frequency	100 s (Without transients) and 100 Hz
Grid loss through LVRT initiation time	$t = 20$ s

The LVRT event is triggered at $t = 20$ s for all the 12 simulations after first simulating 100 seconds of initialization. Since it is a load case for ultimate load analysis, the maxima of the main bearing loads in addition to the operating temperature (T_B) are given in Figure 28. It was found that the percentage deviation from the mean value for the extreme values are insignificant for the radial loads as in Figure 28(b). Whereas the deviation with regards to the maximum value is very high for both axial loads F_a and the bearing temperature using T_B as in Figure 28(d) and Figure 28(f). The simple temperature model used to predict the bearing temperature is described in Deliverable report D5.1. The difference between average values and the extreme values is high for the above rated wind speeds since the drop in the generator torque T_g is very high during the LVRT action in these wind speed regimes above rated wind speed.

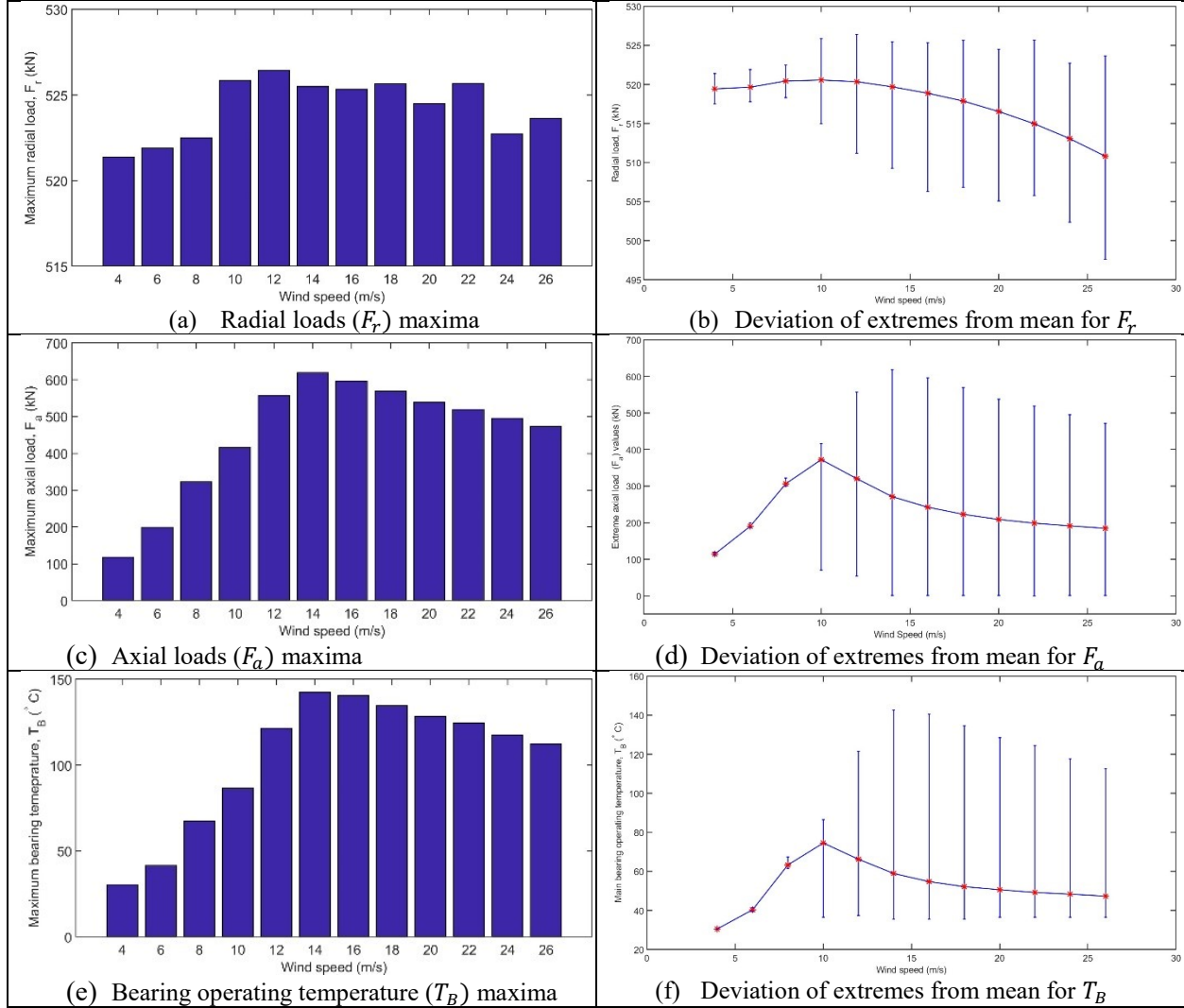


Figure 28: Maxima of main bearing loads and the operating temperature (T_B) under DLC 2.5

8.2.1. Allowable bearing static equivalent load during LVRT

Given the static load safety factor of $S_0 = 3$ [26] and the basic static load rating (radial) $C_{0r} = 21200$ kN for the FAG 230/800 bearing [27], the allowable static equivalent load is calculated as [26],

$$P_{0,allowed} = \frac{C_{0r}}{S_0} = \frac{21200 \text{ kN}}{3} = 7066.7 \text{ kN} \quad (12)$$

The actual maximum impact load that occurs during the wind turbine operation undergoing a Low Voltage Ride Through event for each mean wind speed is obtained by [26],

$$P_{0,actual} = X_0 \cdot F_{r,max} + Y_0 \cdot F_{a,max} \quad (13)$$

Where static radial load factor $X_0 = 1$ and $Y_0 = 3$ for the FAG 230/800 bearing [27].

Figure 29 is showing the ratio between the allowable static equivalent load of the Teesside main bearing and actual static equivalent load as obtained from (12) and (13) applied to Figure 28. It seems that the allowable loads are always about a factor of 2.5 to 3 higher than the safety factor required to be 3. This

implies that the LVRT does not lead to permanent deformations in the roller-raceway contact surfaces of the Teesside main bearing.

Besides the comparison of the extreme load during the Low Voltage Ride Through (LVRT) event it should also be noted a considerable temperature increase up to $T_B \approx 145 \text{ }^\circ\text{C}$ is predicted using the simple temperature model of D5.1. This is well below the maximum temperature limit $T_{max} = 200 \text{ }^\circ\text{C}$ of the FAG 230/800 main bearing and it is concluded that the LVRT events are not expected to cause overheating of the bearing. It should be noted that the simple temperature model of D5.1 is very likely overestimating the transient bearing temperature, since the specific heat of the bearing steel is not included in the temperature model, which is only ensuring a heat transfer balance between the friction heat of the bearing and the convection cooling at the outer surface of the bearing. It should however be noted that the main bearing grease being represented by Klüberplex BEM 41-301 as described in the HIPERWIND deliverable D5.1 has a specified maximum upper service temperature of $120 \text{ }^\circ\text{C}$, which will be violated by the predicted $T_B \approx 145 \text{ }^\circ\text{C}$ shown above. A considerable degradation of the grease is expected if heated too much and the contamination level of the grease is then expected to chance afterwards. It is however believed that the predicted bearing temperature is overestimated and that the specific heat of the main bearing steel will limit the temperature increase during the short Low Voltage Ride Through. It should on the other hand be considered as a possible cause for grease degradation and for the need of replacing the grease more often than initially predicted.

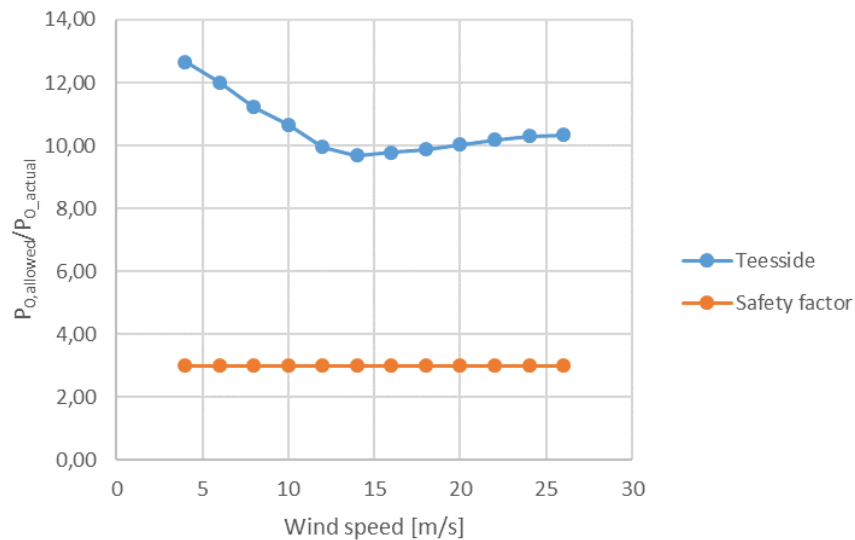


Figure 29 Estimate of the Teesside SWT 2.3 – 93 m main bearing actual static equivalent load compared to the allowable static equivalent load when undergoing a Low Voltage Ride Through (LVRT) event at different wind speeds and a turbulence intensity of 0.16 according to the IEC design wind class IA. A safety factor of $S_0 = 3$ is recommended by Schaeffler and this is exceeded by almost a factor of 3 for all wind speeds.

8.3. Combining Low Voltage Ride Through events with normal production load cases

In order to evaluate the fatigue impact of the Low Voltage Ride Through (LVRT) event investigated for the Teesside wind farm in terms of the Design Load Case DLC 2.4 “Power production with loss of electrical network”, then the event statistics as illustrated in Figure 7 is compared to the fatigue impact of the load cases imposed by the wind environment as reported in the Hiperwind deliverable report D5.1. The environmental impact in terms of wind speed distribution and turbulence intensity was investigated in the Design Load Case 1.2 “Normal Production” as well as the DLC 3.1 “Start-up” and DLC 4.1 “Normal shutdowns”. Table 5 is summarizing the duration of the design load case DLC 2.4 along with the load cases of the D5.1 as well as the estimate modified L_{10mt} lifetime of the design load cases.

The total resulting L_{10mT} lifetime of the Teesside wind farm main bearings including the fatigue load cases is calculated by eq.(14) below, when inserting the duration and lifetime of the specific load cases.

Table 5 Combining the load cases of the Teesside wind farm into by accounting for the fraction of a year that they are represented in the operation of the wind farm.

Design Load Cases & Durations	Total number of hours in a year $365 \frac{\text{days}}{\text{year}} \cdot 24 \frac{\text{hour}}{\text{day}} = 8760 \text{ hours/year}$
DLC 2.4 Power production with loss of electrical network. The expected number of event is 10 times per year as shown in Figure 7 with a duration of 100 sec simulation.	0.28 hours = 1000 seconds ($P_{DLC24} = 0.0032 \%$) $L_{10mt,DLC24} = 92 \text{ years}$
DLC 3.1 Start-up Duration of startup events (DLC 3.1) in a year as per IEC 61400-1 [25](1000 startup-procedures at 4 m/s., 50 start-up procedures each at 12 m/s and 26 m/s with a duration of 100 s)	30.56 hours ($P_{DLC31} = 0.35 \%$) $L_{10mt,DLC31} = 223 \text{ years}$
DLC 4.1 Normal shutdown Duration of shutdown events (DLC 4.1) in a year as per IEC 61400-1 [25] (1000 shutdown procedures at 4 m/s., 50 shutdown procedures each at 12 m/s and 26 m/s with a duration of 100 s).	30.56 hours ($P_{DLC41} = 0.35 \%$) $L_{10mt,DLC41} = 39591 \text{ years}$
DLC 1.2 Normal power production Duration of DLC 1.2 obtained by assuming that the wind turbine operated under DLC 1.2 for the remaining hours in a year.	8698.7 hours ($P_{DLC12} = 99.3 \%$) $L_{10mt,DLC12} = 42 \text{ years}$

$$L_{10mT} = \frac{(P_{DLC24} + P_{DLC31} + P_{DLC41} + P_{DLC12})}{\left(\frac{P_{DLC24}}{L_{10mt,DLC24}} + \frac{P_{DLC31}}{L_{10mt,DLC31}} + \frac{P_{DLC41}}{L_{10mt,DLC41}} + \frac{P_{DLC12}}{L_{10mt,DLC12}}\right)} \quad (14)$$

$$= \frac{(3.2 \cdot 10^{-5} + 3.5 \cdot 10^{-3} + 3.5 \cdot 10^{-3} + 0.993)}{\left(\frac{3.2 \cdot 10^{-5}}{92 \text{ year}} + \frac{3.5 \cdot 10^{-3}}{223 \text{ year}} + \frac{3.5 \cdot 10^{-3}}{39591 \text{ year}} + \frac{0.993}{42 \text{ year}}\right)} = 42.3 \text{ year}$$

Where P_{DLCXX} is the duration and $L_{10mt,DLCXX}$ is the life time of the load case XX, with XX = 24, 31, 41 or 12.

It is seen from eq. (14) that the total fatigue life of the Teesside main bearings when combining the Design Load Case 2.4 with DLC 3.1, 4.1 and 1.2 is found to be 42.3 years, which is basically the same life time of 43.3 years as was found in the deliverable D5.1 when combining only the 3 last design load cases. It is now interesting to review the formulation of the design load case 2.4 “Power production plus occurrence of fault” plus “Control system fault, electrical fault or loss of electrical network”:

Design Load case 2.4 comment on page 46 of IEC 61400-1 Ed 4 (2019) :

“If a fault or loss of electrical network connection does not cause an immediate shutdown and the subsequent loading can lead to significant fatigue damage, the likely duration of this situation along with the resulting fatigue damage in normal turbulence conditions (NTM) shall be evaluated in DLC 2.4. The manufacturer shall estimate the expected frequency/duration for the events⁷.”

Where comment ⁷ states the following:

“⁷If there is no relevant data/information available, the following frequency/duration can be applied for the below listed events:

- 10 shut-downs per year for overspeed event;
- 24 hours per year of operation for events with yaw error;
- 24 hours per year of operation for events with pitch error;
- 20 times per year with loss of electrical network connection”

First of all, the frequency of the loss of electrical network connection of the Teesside wind farm is found to be 10 events per year in Figure 7, which is half of what is specified in the IEC 61400-1 standard, but in a similar order of magnitude. When returning to the comment for DLC 2.4 then the fatigue analysis of the LVRT events of the Teesside wind farm has shown that this is NOT causing any “significant fatigue damage” of the main bearing. It can therefore be concluded that DLC 2.4 has been investigated for the main bearing of the Teesside wind farm and with a positive outcome that no significant fatigue damage is expected.

9. Discussion

Despite well-established grid disturbance countermeasures for WTG in GCs, the potential impacts on the structure and electrical system remain unclear. While various control architectures have been proposed in literature to mitigate such disturbances, industry and academia have yet to thoroughly examine the effects of these actions in terms of life reduction or maximal loading capacity. This lack of information is particularly apparent for type 4 WTG, with limited publicly available data. To validate the results of this report, similar studies on type 3 WTG were reviewed. Despite their different concepts, both face similar requirements from Grid Codes and design driving events.

An examination of the Low Voltage Ride Through (LVRT) impact in terms of only the radial degrees of freedom in a 5 MW gearbox was examined by Gallego-Calderon *et. al.* for the NREL 5 MW reference turbine [19]. The simulations showed that the short duration LVRT specification of the grid code of Quebec did have the largest impact in term of exciting torsional modes in the drive train and that the extreme load limit of the planet bearing could be exceeded, if the bearing was choosen too small. The generator torque is reported to increase to 175 % of the rated torque due to the LVRT event. This is considerably higher than what has been observed in the study presented here and is believed to reflect the difference between a Type 3 and Type 4 drive trains configuration.

A detailed analysis of the impacts of LVRT on the structure of a Type 3 DFIG 2 MW turbine was carried out by Arbeiter *et. al.* in [28]. It is worth noting that the impact on a type 3 DFIG is more severe due to its stator being directly connected to the grid, meaning that all grid dynamics propagate to the generator and rotor regardless of the control technique employed. Arbeiter *et. al.* found that the LVRT controller implemented in the grid-side converter produced an overspeed of the turbine rotor, which was successfully controlled by the pitch controller. The measurements showed maximal values of 110% of the nominal, varying depending on voltage dip characteristics and wind conditions. The simulations of this report found rotor over speeds reaching 40 % when the wind speed is above rated wind, since the pitch controller is responding to the lack of power output. Below rated wind speed the over speeding is very reduced. It is suggested to check if this over speeding of the turbine rotor will result in blade loads exceeding the design limit, but it is not clear if the blade design is available for such an examination.

In terms of torque behavior, Arbeiter *et. al.* found that the maximal torque of 140% was produced by a combination of mean airgap torque and peak oscillation of the inertial torque produced by the mode excitation of the drive train. Although the simulations of this report also showed some mode excitation, this had no preponderant effect on torque behavior, possibly due to differences in the drive train. Nonetheless, our maximal values showed an increase in torque in the range of 15 % during and after the LVRT event.

The main difference between the Type 3 turbine results of the literature and the Type 4 turbine simulations reported here seems to be a significant lower excitation of the torque modes of the drive train and significant lower torque loads. It will be interesting to investigate further if measurements from the Teesside wind farm can confirm this. A second large difference is a larger over speeding at the LVRT of the current Type 4 turbine simulations, since no LVRT control scheme of the pitch controller has been implemented. Again, comparing with the response of the Teesside wind turbines could clarify if that is needed to replicate the loads of the SWT 2.3 – 93 turbines.

10. Conclusion

In order to ensure that wind turbines are able to perform a Low Voltage Ride Through (LVRT), where the turbine stays connected to the grid in case of short voltage drops, then one has to be able to represent the LVRT event in wind turbine load simulations. In this report an aeroelastic load simulation model in the HAWC2 software has been combined with a Simulink model of a type 4 drive train to represent the SWT 2.3 – 93 turbines of the Teesside wind farm operated in the UK in the context of examining, if the life of the main bearing of the turbines will be significantly affected by the LVRT events of the windfarm. The life model of the main bearing has been reported in the HIPERWIND project deliverable 5.1 and forms the basis for the evaluation and the aeroelastic model description in relation to the life model as formulated in ISO 281.

The Simulink model of the Type 4 drive train has included the action of activating a chopper resistor across the capacitor of the DC link in the power converter as means to limit the voltage of the DC link as the grid is lost as described by the grid code. This scheme could in principle be used to perform a LVRT, where the generator will experience no disturbance, but in order to reduce the heat load of the chopper resistor it is proposed to ramp down the generator current and thereby the torque after the first activation of the chopper. This scheme has been evaluated on the Teesside wind turbines by calculating the load time series for the IEC Design Load Cases 2.4 “Power production with loss of electrical network” and 2.5 “Power production with Low Voltage Ride Through”.

It has been found that about 10 LVRT events per year is the average level of the Teesside wind farm and the impact on fatigue in terms of the LVRT assigned to IEC DLC 2.4 can be concluded to be insignificant in terms of the main bearing lifetime. Secondly the extreme loads on the main bearing due to the LVRT according to IEC DLC 2.5 have been found to be lower than the allowed loads by a factor of almost 10 and thereby complying with the demand of a safety factor of 3 for the main bearing.

Investigation of the life models of other drive train components like the gearbox have not been performed due to lack of public available information about Teesside gearbox internal details

11. Outlook

Future work could be done by expanding the analysis to more drivetrain components like the gearbox, but this will call for detailed information about the gearbox internal components, like bearings, shaft dimensions and thickness of the gearbox housing supporting the bearings. It has not been possible to find publicly available gearbox information with sufficient details to perform such an analysis, but it could be considered, if companies involved in repairing gearboxes for wind turbines could provide information about refurbished gearboxes in order to evaluate the impact of the LVRT on the gearbox internals.

Further more, it is proposed to identify a LVRT event of the Teesside wind farm in order to validate the LVRT simulation model and to investigate if the torque, speed and pitch profiles during the LVRT of this report are similar to the observed profiles of the Teesside wind farm.

Bibliography

- [1] M. Singh and S. Santoso, "Dynamic Models for Wind Turbines and Wind Power Plants," NREL, Austin, Texas, 2011.
- [2] E. Coster, A. Ishchenko, J. Myrzik and W. Kling, "Modeling, Simulating and Validating Wind Turbine Behavior During Grid Disturbances," IEEE Power Engineering Society General Meeting 2007, pp. 1-6, doi: 10.1109/PES.2007.386110., 2007.
- [3] A. D. Hansen, N. A. Cutululis, H. Markou, P. E. Sørensen and F. Iov, "Grid fault and design-basis for wind turbines - Final report," Danmarks Tekniske Universitet, Risø Nationallaboratoriet for Bæredygtig Energi, Denmark. Forskningscenter Risøe. Risøe-R No. 1714(EN), 2010.
- [4] S. Achilles and M. Pöller, "Direct Drive Synchronous Machine Models for Stability Assessment of Wind Farms," DIgSILENT GmbH, 2003.
- [5] O. S. Senturk and A. M. Hava, "A Simple Sag Generator Using SSRs," *IEEE Transactions on Industry Applications*, vol. 48, no. 1, pp. 172-180, 2012.
- [6] Y. Han, Y. Feng and P. Yang, "Cause, Classification of Voltage Sag, and Voltage Sag Emulators and Applications: A Comprehensive Overview," *IEEE Access*, vol. 8, pp. 1922-1934, 2020.
- [7] M. Bollen, "Characterisation of voltage sags experienced by three-phase adjustable-speed drives," *IEEE Transactions on Power Delivery*, vol. 12, no. 4, pp. 1666 - 1671, 1997.
- [8] X. Yan, L. Yang and T. Li, "The LVRT Control Scheme for PMSG-Based Wind Turbine Generator Based on the Coordinated Control of Rotor Overspeed and Supercapacitor Energy Storage," *Energies* 2021, 14, 518. <https://doi.org/10.3390/en14020518>.
- [9] "thewindpower," [Online]. Available: https://www.thewindpower.net/windfarm_en_6353_teesside.php. [Accessed 01 Jan 2023].
- [10] Y. Tyllinen, "PERFORMANCE DATA OF GENERATOR," ABB OY, 2002.
- [11] Z. E. Recordon, "Tecnología de punta en aerogeneradores," in *cigre chile*, 2009.
- [12] SIEMENS, *Product Catalog SWT-2.3-93*.
- [13] F. Iov, A. D. Hansen, P. E. Sorensen and N. A. Cutululis, "Mapping of grid faults and grid codes," Risø National Laboratory, 2007.
- [14] P. Kundur, *Power System Stability and Control*, Palo Alto, California: McGraw Hill, Inc., 1993.
- [15] N. Kroutikova, H.-A. C. A. and T. C. Green, "State-space model of Grid-connected inverters under current control mode," *IET Electric Power*, vol. 1, no. 1, pp. 329-339, 2007.
- [16] T. Larsen and A. M. Hansen, "How 2 HAWC2, the user's manual," Risø-R-1597(ver.4-5)(EN). Risø National Laboratory, Technical University of Denmark., 2014.

- [17] B. B. Garzón, "Integrated analysis of wind turbines - The impact of power systems on wind turbine," Technical University of Denmark, 2012.
- [18] J. Gallego-Calderon, "Electromechanical Drivetrain Simulation," 2015.
- [19] J. Gallego-Calderon, A. Natarajan and N. A. Cutululis, "Ultimate design load analysis of planetary gearbox bearings under extreme events," *Wind Energy*, vol. 20, pp. 325-343, 2017.
- [20] M. H. Hansen and L. C. Henriksen, "Basic DTU Wind Energy controller," DTU Wind Energy, Roskilde, 2013.
- [21] IEC 61400-3-1, "Wind energy generation systems - Part 3-1: Design requirements for fixed offshore wind turbines," International Electrotechnical Commission (IEC), Geneva, 2019.
- [22] S. Wang, A. R. Nejad, E. E. Bachynski and T. Moan, "Effects of bedplate flexibility on drivetrain dynamics: Case study of a 10 MW spar type floating wind turbine," *Renewable Energy*, vol. 161, p. 808–824, 2020.
- [23] ISO 281, "Rolling Bearings: Dynamic Load Ratings and Rating Life," International Organization for Standardization, Geneva, 2007.
- [24] ASTM D341-20e1, "Standard Practice for Viscosity-Temperature Equations and Charts for Liquid Petroleum or Hydrocarbon Products," ASTM International, West Conshohocken, 2020.
- [25] IEC 61400-1 Ed. 4, "Wind energy generation systems –Part 1: Design requirements," International Electrotechnical Commission (IEC), Geneva, 2019.
- [26] Schaeffler, "Load carrying capacity and life," Schaeffler, [Online]. Available: <https://medias-at.schaeffler.com/en/load-carrying-capacity-and-life#20516346507>. [Accessed 10 March 2023].
- [27] F. Schaeffler, "FAG 230/800-MB," [Online]. Available: <https://medias.schaeffler.nl/en/product/rotary/rolling-and-plain-bearings/roller-bearings/spherical-roller-bearings/spherical-roller-bearings/230/800-mb/p/389661#Product%20Information>. [Accessed 10 March 2023].
- [28] M. Mathias Arbeiter, M. Hopp and M. Huhn, "LVRT Impact on Tower Loads, Drivetrain Torque and Rotational Speed—Measurement Results of a 2-MW Class DFIG Wind Turbine," *Energies*, vol. 14, no. 3539, 2021.
- [29] PowerFactory 2021, "DIgSILENT Battery Energy Storage System," *PowerFactory Technical Reference*, 2021.
- [30] IEC 61400-1, "Wind energy generation systems - Part 1: Design requirements," IEC, Geneva, Switzerland, 2019.

Appendix A

In order to calculate the standard synchronous model parameters of the 6th degree model provided in section 5, the following equations have been used. All data here used has been translated in to p.u. system.

Parameter Name	Symbol	Value
Synchronous reactance (saturated, unsat)	X_d	0.670 0.97
Negative phase sequence synchronous reactance	X_-	0.041
Negative phase sequence synchronous resistance	R_-	0.003
Positive phase sequence synchronous reactance	X_+	0.084
Positive phase sequence synchronous resistance	R_+	0.161
Zero phase sequence reactance 2)	X_0	N.A. -
Zero phase sequence resistance 2)	R_0	N.A. -
Direct axis transient open circuit time constant	T'_{d0}	1.519 s
Subtransient open circuit time constant	T''_{d0}	0.013 s
Direct axis transient short circuit time constant	T'_d	0.081 s
Subtransient short circuit time constant	T''_d	0.012 s
Armature time constant	T_a	0.042 s
Locked rotor power factor	-	0.12
Open circuit saturation curve points 3)	$S(1.0)$	1.42
Open circuit saturation curve points 3)	$S(1.2)$	2.24
Inertia constant of generator	H	0.294 kW/s/kVA

$$F_{nom} = 50;$$

$$\omega_n = 2 * \pi * F_{nom};$$

$$x_{ad} = x_d - x_l;$$

$$x_{aq} = x_q - x_l;$$

$$x_1 = x_d - x_l + x_{rld};$$

$$x_2 = x_1 - \frac{(x_d - x_l)^2}{x_d};$$

$$x_3 = \frac{(x_2 - x_1 * \frac{x_{dpp}}{x_d})}{(1 - \frac{x_{dpp}}{x_d});}$$

$$T_1 = \frac{x_d}{x_{dp}} * t_{dp} + \left(1 - \frac{x_d}{x_{dp}} + \frac{x_d}{x_{dpp}}\right) * t_{dpp};$$

$$T_2 = t_{dp} + t_{dpp}; a = \frac{x_2 * T_1 - x_1 * T_2}{x_1 - x_2};$$

$$b = x_3 - (x_3 - x_2) * t_{dp} * t_{dpp};$$

$$T_{sigfd} = -\frac{a}{2} + \sqrt{\frac{a^2}{4} - b};$$

$$T_{sigld} = -\frac{a}{2} - \sqrt{\frac{a^2}{4} - b};$$

$$x_{fd} = \frac{(T_{sigfd} - T_{sigld})}{\left(\frac{T_1 - T_2}{x_1 - x_2} + \frac{T_{sigld}}{x_3}\right)};$$

$$x1d = \frac{(Tsig1d - Tsigfd)}{\left(\frac{T1 - T2}{x1 - x2} + \frac{Tsigfd}{x3}\right)}$$

$$rfd = \frac{xfd}{wn * Tsigfd}$$

$$r1d = \frac{x1d}{wn * Tsig1d}$$

$$x1q = (xq - xl) * \frac{xqpp - xl}{xq - xqpp}$$

$$r1q = xqpp/xq * (xq - xl + x1q) / (wn * tqpp)$$

$$L = \begin{bmatrix} 1.2 & 0 & 0 & 0 & 1.142 \\ 0 & 3.65 & 3.592 & 3.592 & 0 \\ 0 & 3.592 & 3.7367 & 3.592 & 0 \\ 0 & 3.592 & 3.592 & 4.5595 & 0 \\ 1.142 & 0 & 0 & 0 & 1.143 \end{bmatrix}; R = \begin{bmatrix} 0.0081 & 0 & 0 & 0 & 0 \\ 0 & 0.0081 & 0 & 0 & 0 \\ 0 & 0 & 0.0079 & 0 & 0 \\ 0 & 0 & 0 & 0.2667 & 0 \\ 0 & 0 & 0 & 0 & 0.149 \end{bmatrix}$$

Appendix B

Inverter and Electric grid Parameters

Kifr	Integral gain for voltage regulation	20
Kpfr	Proportional gain for voltage regulation	8
KiTE	Integral gain for Te regulation	1
KpTE	Proportional gain for Te regulation	3
KIRT	LVRT fast control integral gain	200
KpRT	LVRT fast control proportional gain	30
Kid	Integral gain current control	2
Kpd	Proportional gain current control	20
KiVAC	Integral gain Vac control	1
KpVAC	Proportional Vac control	3
KiDC	Integral gain Vdc control	10
KpDC	Proportional Vdc control	3
kiQ	Integral gain reactive power control	10
KpQ	Proportional reactive power control	3
Rgrid	Aggregated Grid equivalent resistance	0.01 p.u.
Lgrid	Aggregated Grid equivalent inductance	0.1 p.u.
Rtrafo	Equivalent transformer resistance	0.001 p.u.
Ltrafo	Equivalent transformer inductance	0.15 p.u.
DC capacitor	DC link capacitor	0.054 F